nature communications

Article

https://doi.org/10.1038/s41467-025-59617-1

A minimally invasive thrombotic model to study stroke in awake mice

Received: 21 April 2024

Accepted: 29 April 2025

Published online: 10 May 2025

Check for updates

Kimberly Marks, Sung-Ji Ahn, Ninamma Rai, Antoine Anfray, Costantino Iadecola & Josef Anrather

Experimental stroke models in rodents are essential for mechanistic studies and therapeutic development. However, these models have several limitations negatively impacting their translational relevance. Here we aimed to develop a minimally invasive thrombotic stroke model through magnetic particle delivery that does not require craniotomy, is amenable to reperfusion therapy, can be combined with in vivo imaging modalities, and can be performed in awake mice. We found that the model results in reproducible cortical infarcts within the middle cerebral artery (MCA) territory with cytologic and immune changes similar to that observed with more invasive distal MCA occlusion models. Importantly, the injury produced by the model was ameliorated by tissue plasminogen activator (tPA) administration. We also show that MCA occlusion in awake animals results in bigger ischemic lesions independent of day/night cycle. Magnetic particle delivery had no overt effects on physiologic parameters and systemic immune biomarkers. In conclusion, we developed a novel stroke model in mice that fulfills many requirements for modeling human stroke.

Stroke is a leading cause of death and disability worldwide, with a stroke occurring every 40 s in the United States alone[1]. Of these, roughly 87% are ischemic, in that brain damage occurs from a clot blocking a major cerebral artery, most commonly the middle cerebral artery (MCA)[2,3]. The standard strategies for reperfusion in acute ischemic stroke include early delivery of recombinant tissue plasminogen activator (tPA) or endovascular thrombectomy, both of which must be performed within hours of a stroke, thus preventing most patients from ever receiving effective treatment[4]. Furthermore, in roughly 50% of cases, arterial recanalization does not improve functional outcomes (futile reperfusion)[5–9].

Improving upon these existing therapies or developing new ones requires robust stroke models that best recapitulate the human disease. Unfortunately, the various models of MCA occlusion currently available fall short of this goal. The reasons for this include: (a) the production of large infarcts encompassing brain areas outside the MCA territory typically not affected in human strokes, (b) the need for anesthesia, (c) absence of endogenous and/or therapeutic reperfusion, (d) sudden recanalization not reflecting the gradual clot dissolution and reperfusion observed in humans, (e) poor intravital imaging compatibility, and (f) the need for a craniotomy to expose the MCA, which interferes with post-ischemic inflammatory processes and alters CBF dynamics[10,11].

Here we describe a novel minimally invasive model of reversible MCA occlusion in mice using intravenously injected thrombin-coated magnetic particles combined with a micro-magnet placed over the intact skull overlying the MCA. We show that this model exhibits several desirable features, including applicability to awake mice, no requirement for anesthesia during MCA occlusion, slow spontaneous reperfusion akin to that seen in humans, no craniotomy, no inflammatory contribution, easy compatibility with 2-photon brain imaging, and reperfusion with tPA[12–15]. This model is well poised to enable advances in stroke pathobiology, for example, the study of circadian effects on stroke outcome and minimizing limitations related to the confounding effects of anesthetics and craniotomy, well-known translational barriers in preclinical stroke research[16,17].

Feil Family Brain and Mind Research Institute, Weill Cornell Medicine, New York, NY, USA. e-mail: joa2006@med.cornell.edu

Results

MCA occlusion by magnetic nanoparticles with endogenous reperfusion

Following a study that used a non-invasive method of reversible MCA occlusions using magnetized nanoparticles[18], we aimed to develop a stroke model in mice that would reproducibly generate an 85% or greater drop in cerebral blood flow (CBF) necessary to induce ischemic brain injury[14]. To accomplish this, we placed an attractive magnet over the temporal bone while simultaneously injecting magnetic particles into venous circulation (Fig. 1). A temporary ligation of the ipsilateral common carotid artery (CCA) was necessary to allow for reproducible aggregation of particles at the MCA (Fig. 1a, c). The particles (180 nm) used by Jia et al.[18] did not provide the desired 85% or greater decrease in CBF to the MCA as shown by Laser Doppler Flowmetry (Fig. 1c). Larger particles (500 nm) provided a drop >85% in CBF. However, upon removal of the attractive magnet, reperfusion occurred immediately due to the particles re-entering circulation. This pattern of ischemia/reperfusion is similar to that obtained in the intraluminal filament model, in which reperfusion occurs immediately upon removal of the filament[14]. To better mimic the gradual endogenous reperfusion observed in patients with ischemic stroke[12,13], we designed custom magnetic nanoparticles with greater occlusive power. Bovine serum albumin (BSA) coated particles (500 nm) were conjugated to bovine thrombin to form thrombin coated magnetic particles (tMP) (Supplementary Fig. 1a). Eight units of thrombin/mg particles were found to be the limit at which no added thrombin would confer additional potency as determined by a plasma coagulation assay (Supplementary Fig. 1b). Using these tMP, an 85% or greater drop in CBF was observed with the added benefit of a more stable occlusion and gradual reperfusion after magnet removal (Figs. 1c, 2). Longitudinal studies using laser speckle imaging (LSI) revealed reperfusion occurring gradually over several days, matching the perfusion level of the contralateral MCA territory by day 5 after occlusion (Fig. 2a). No CBF reduction was observed in sham animals that underwent the same surgical procedure and tMP injection, without magnet placement apart from the expected roughly 25% CBF decrease from the carotid ligation (Fig. 2b). Infarct volumes 48 h post-stroke showed a cortical lesion mean ± SEM of 11.5 ± 1.9 mm^3 (Fig. 1d, e), while no injury was observed in sham animals. tPA given intravenously 35 min after occlusion resulted in recanalization of the occluded MCA, leading to rapid CBF restoration to near baseline levels and in significantly smaller injury (2.7 ± 2.2 mm^3) (Fig. 1e). No significant difference in infarct volumes was observed when comparing male and female mice (Supplementary Fig. 2).

Particle body distribution, impact on blood chemistry, and inflammatory markers

Next, we used body and brain T2-weighted MRI imaging of sham mice injected with tMP or saline and tMPS (stroke) mice to determine the fate of the particles. Particles were found largely in the liver 1 h post injection (Supplementary Fig. 1c). Hyperechoic intensity in the brain resulting from accumulation of magnetic particles to the MCA and areas of cortical injury were captured by coronal MRI (Supplementary Fig. 1d). Given the accumulation of tMP in the liver as evidenced by MRI, we performed histologic studies of liver tissue 1 h and 4 weeks after tMP delivery (Supplementary Fig. 3). The analysis showed that nanoparticles were localized within cells located in the venous liver sinuses but not in the parenchyma or bile ducts. The cells are likely Kupffer cells, which have been shown to constitute a major clearing route for intravenously delivered nanoparticles[19,20]. Particles were highest at 1 h after delivery, but remained detectable, albeit significantly decreased, at 4 weeks after delivery (Supplementary Fig. 3b). We did not find any signs of hepatic cell death, immune cell infiltration, or tissue remodeling (e.g., fibrosis). To determine the impact of the particles on liver function, we assessed serum alkaline phosphatase, alanine transaminase, aspartate aminotransferase, total protein, triglyceride, and total bilirubin at 48 h, 7 days and 14 days following tMPS and in sham-treated mice (Supplementary Fig. 4a). No statistically significant differences were found in groups between days except for ALP showing a moderate decrease in sham tMP and tMPS groups. Arterial pH, pCO_2, pO_2, and mean arterial pressure measured before and immediately after tMPS and tMP sham surgery showed no statistical difference between groups except for a slight rise in pH in the tMP group (Supplementary Fig. 4b). pH, pCO_2, and pO_2 were all within normal physiologic ranges for tMPS and tMP sham[21].

To rule out systemic inflammation resulting from tMP, selected serum cytokines known to be regulated in ischemic stroke were measured at 4, 24, 48 h, and 7 days following tMPS, tMP sham surgery, or saline-treatment[22–25]. As expected, given the inflammatory sequelae of stroke, serum cytokines were increased in tMPS when compared to control groups (Supplementary Fig. 4c)[22,23,26]. No differences were found between tMP sham and saline sham groups. We conclude that the tMP themselves do not elicit a systemic inflammatory response that could aberrantly contribute to ischemic injury and recovery, and that any significant impact on systemic inflammatory markers results from the ischemic injury itself.

Behavioral deficits after tMP stroke

Given that the somatosensory cortex is the major brain area targeted by distal MCA occlusion, we performed neurobehavioral tests that predominantly test the function of this brain region[27]. Wire hanging measures grip strength, balance, and endurance with the behavioral output as latency to fall from the suspended wire[28]. Mice receiving tMPS had shorter times suspended when compared to tMP sham groups, a deficit that could be rescued by therapeutic doses of tPA (Fig. 3a). The corner test detects sensory and motor asymmetries related to barrel cortex outputs, limb coordination, and postural biases[29]. Mice receiving tMPS had an 80% preference to turn right, ipsilateral to the side of the infarct. These findings were statistically significant compared to tMP sham animals and could also be rescued using tPA (Fig. 3b). The adhesive removal test is used to assess cortical damage and coordination deficits[30]. At 3 days following injury, mice receiving tMPS had increased latency to contact the adhesive attached to the paw and increased time to remove adhesive when compared to the tMP sham group (Fig. 3c).

tMP stroke results in immune cell infiltration in the neocortex

Neuronal cell loss, glial activation, and immune responses of brain-resident and peripheral immune cells are hallmarks of stroke pathology[26,31,32]. To visualize cytologic changes induced by tMPS, we performed qualitative immunocytochemistry 48 h post stroke showing axonal, microglial, and astrocytic changes (Supplementary Fig. 5a). MAP-2 staining showed axon depletion in the infarct core, Iba-1 staining showed a reduction of microglia/macrophages in the core, while GFAP-positive astrocytes were increased in the peri-infarct region at 48 h. Staining of the distal MCA branches using fibrinogen and platelet marker CD41 showed the presence of platelets and fibrinogen in distal branches of MCA 4 h after stroke, with labeling of penetrating vessels in the parenchyma (Supplementary Fig. 5b).

We then used flow cytometry to examine in greater detail the immune cell populations at 1, 2, and 7 days after tMPS and compared them to the uninjured contralateral cortex (Fig. 4). $CD45^{hi}$ infiltrating leukocytes were elevated in the ipsilateral cortex at all time points. No significant changes in $CD45^{int}$ (microglia) and endothelial cells were found over time. $Ly6C^{hi}$ and $Ly6C^{lo}$ monocyte-derived cells (MdC) were elevated at 48 h and $Ly6C^{lo}$ MdC at 7 days. Neutrophils were elevated at 48 h in the ipsilateral cortex. T cells and NK cells were elevated at 7 days when compared to the contralateral cortex. B cells did not differ between groups, but levels trended upwards at 2 days after stroke (Fig. 4).

https://doi.org/10.1038/s41467-025-59617-1

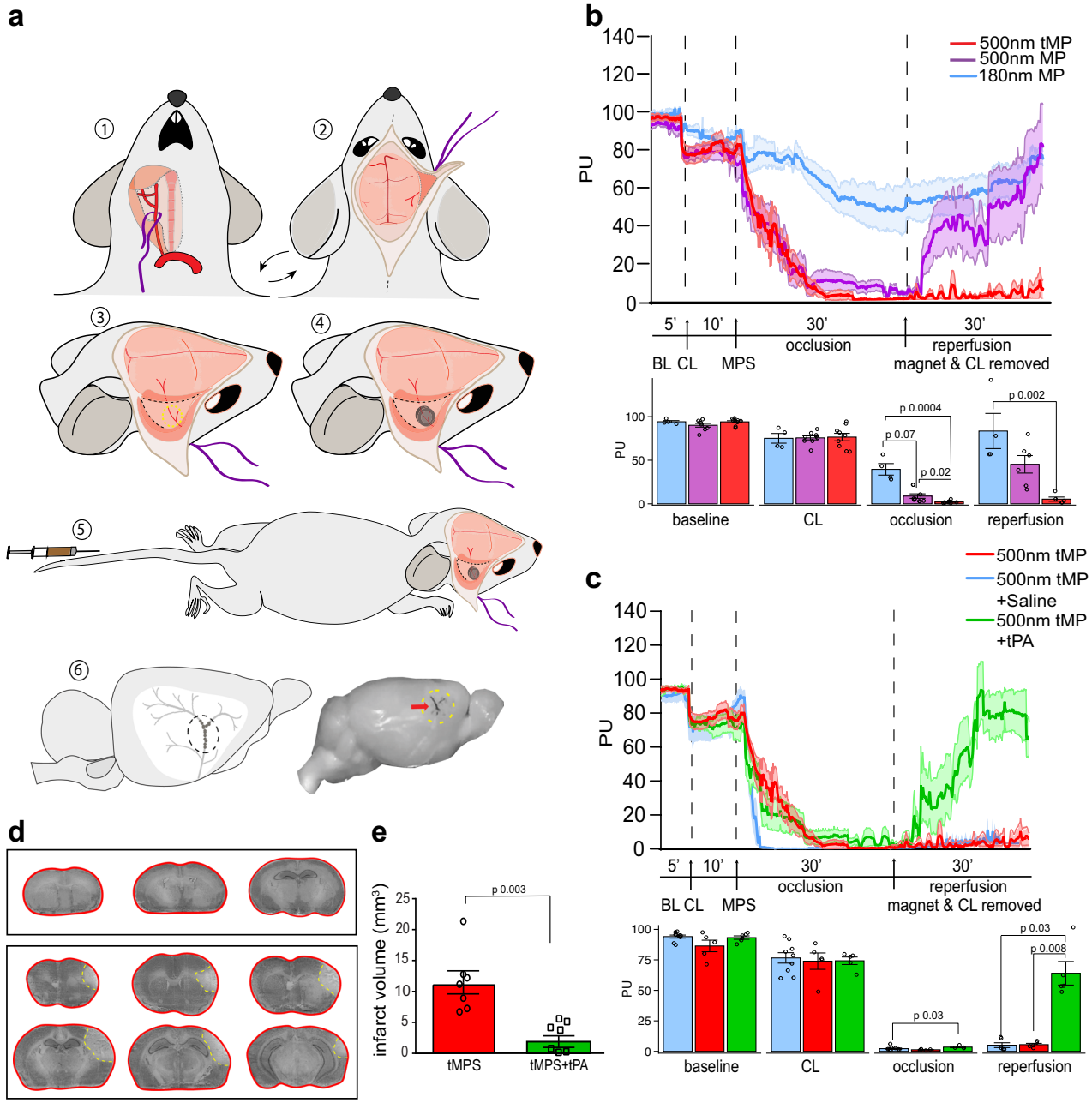

Fig. 1 | Surgical scheme and assessment of magnetic particle stroke. a Surgical strategy for MCA stroke using magnetic particles: (1) Right common carotid artery surgically isolated and held by nylon thread; (2) Animal turned supine and scalp excised to remove right temporal muscle, exposing temporal bone; (3) Thinning of temporal bone to ~70 μm over MCA using burr drill; (4) Placement of magnet over thinned area; (5) Tail vein injection of 250 μl tMP in saline; (6) Accumulation of particles in distal branches of the MCA. **b** Laser Doppler flowmetry measuring relative cerebral blood flow (CBF) changes as perfusion units (PU) in the MCA territory before surgery, following carotid ligation (CL), tMP injection (MPS), 30 min occlusion, and reperfusion after the removal of both magnet and CL. Effect of particle size and composition on LDF (180 nm $n = 4$, 500 nm MP $n = 9$, 500 nm tMP $n = 9$; bar graphs show binned time points. Occlusion and reperfusion groups showing binned data points from final 10 min of recordings). One hundred eighty nanometer particles failed to provide sufficient decrease in CBF. Five-hundred-nanometer particles provided sufficient drop in CBF with immediate reperfusion upon magnet removal. Five-hundred-nanometer thrombin particles (tMP) provide desired sustained drop in CBF following magnet removal. One-way ANOVA with Tukey's post-hoc test or Kruskal–Wallis test with Dunn's post-hoc test as appropriate. Data are presented as mean values ± SEM. **c** LDF trace of 500 nm tMP with and without administration of bolus 10 mg/kg tPA modeling therapeutic reperfusion (500 nm tMPS alone $n = 9$; 500 nm tMP with tPA or saline, $n = 5$). Occlusion and reperfusion groups showing binned data points from final 10 min of recordings. One-way ANOVA with Tukey's post-hoc test or Kruskal–Wallis test with Dunn's post-hoc test as appropriate. Data are presented as mean values ± SEM. **d**, Cresyl Violet staining of 30 μm thick coronal brain sections collected at 300 μm intervals. Infarct outlined in yellow. Top panel is sham (magnet and carotid ligation surgery without particles). **e** Infarct volume at 48 h with and without 10 mg/kg tissue plasminogen activator (tPA). Unpaired two-sided *t*-test ($n = 7$/group). Data are presented as mean values ± SEM. Source data are provided as a Source Data file.

Intravital imaging of tMP stroke

The tMPS procedure can be modified to accommodate a non-invasive thin-skull cranial window and headplate for multiphoton imaging[33–35]. Intravascular flow was assessed by measuring red blood cell velocity using line scanning at baseline, following carotid artery ligation, injection of tMP, removal of magnet and ligation (Supplementary Fig. 6a). Red blood cell velocity slowed down following tMP administration, with the injected particles seen as white specs (Supplementary Fig. 6c). By

https://doi.org/10.1038/s41467-025-59617-1

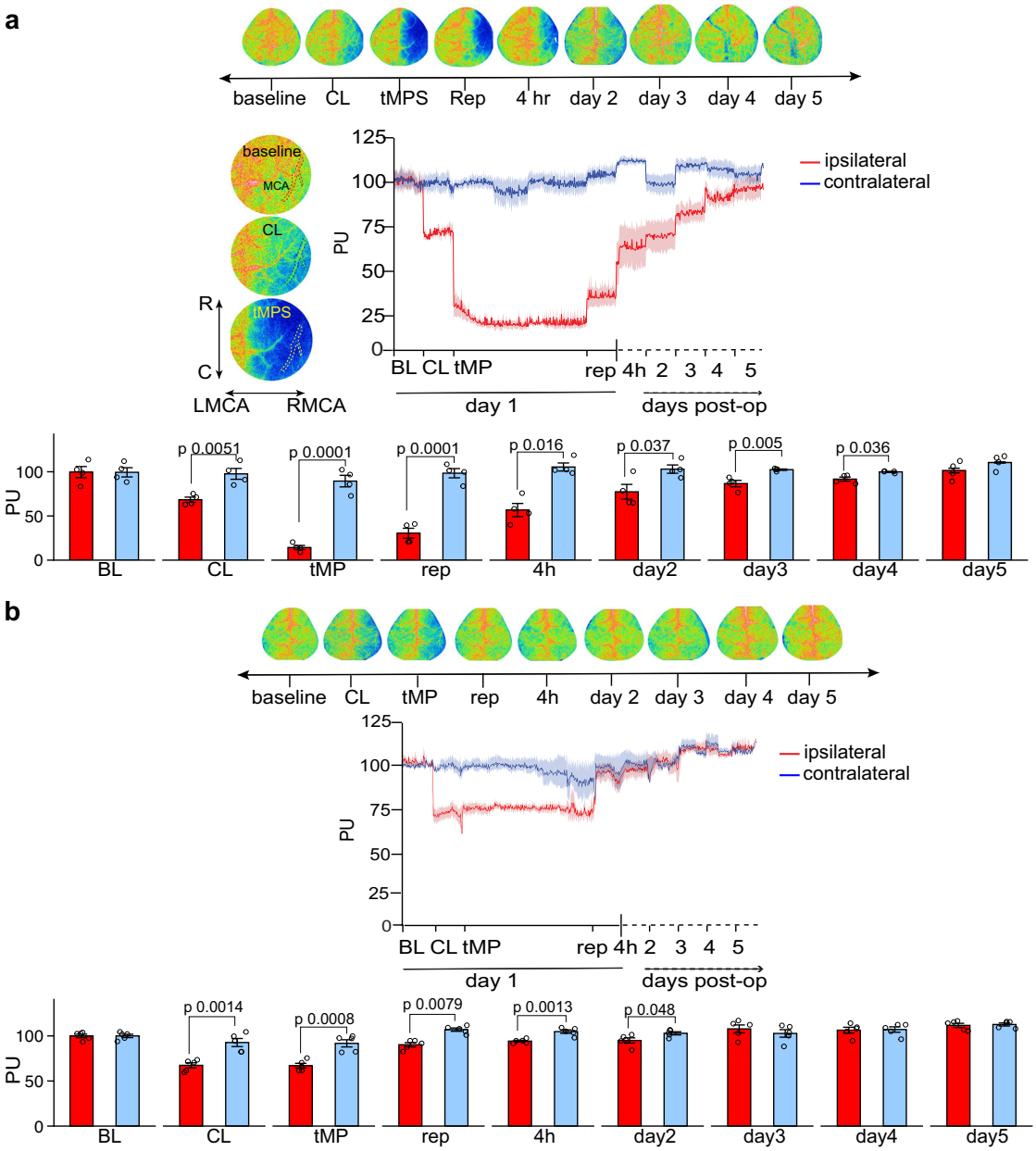

Fig. 2 | Longitudinal perfusion imaging shows endogenous reperfusion after tMP stroke. a Longitudinal Laser Speckle Imaging (LSI) during surgery and 5 days following stroke. Cerebral Blood Flow (CBF) as perfusion units (PU) of ipsilateral and contralateral middle cerebral artery/affected cortex: Baseline (BL) 10 min, CCA ligation (CL) 10 min, tail vein administration of 500 nm thrombin magnetic particles (tMP) 30 min occlusion. Magnet and carotid ligation removed (Reperfusion) 10 min. Values were normalized and binned for last 5 min for all stages, with exception of final 10 min for tMP injection. tMPS shows a gradual increase of CBF to be restored to ipsilateral cortex by day 5; $n = 4$/group, unpaired two-sided t-test. Values are mean ± SEM. **b** Sham surgery and recovery (tMP but no magnet) shows CBF (PU) restored after CL is removed; $n = 5$/group, unpaired two-sided t-test. Values are mean ± SEM. Left of top trace shows zoomed-in representative images with right middle cerebral artery (RMCA) outlined by dashed line. R rostral C caudal, LMCA left middle cerebral artery. Source data are provided as a Source Data file.

20 min and following magnet removal, movement of red blood cells is completely stalled (Supplementary Fig. 6b,c). Diameter measurement of MCA distal branches was decreased during tMPS (Supplementary Fig. 6d). The movies obtained at baseline and following tMP injection (Supplementary Videos 1–5) show the vasodynamic changes of MCA branches downstream of the magnet. Frequent oscillations of constriction and dilation, blood turbulence, and reversal of blood flow were seen in response to tMPS (Supplementary Videos 2 and 3).

tMPS in awake mice

Most models for MCA ischemia/reperfusion in vivo require anesthesia, which is not the case for human stroke[36,37]. Anesthetic agents have a profound impact on the brain and are endowed with neuroprotective effects[16,17]. To eliminate the confounding effect of anesthesia on the development of ischemic brain injury, the tMPS model was adapted to induce strokes in the awake state. To eliminate the need for transient CCA, a micro-coil was placed around the ipsilateral CCA to induce the CBF reduction needed for the microparticles to aggregate and occlude the MCA in the presence of the magnet. This technique also connects the tMP model to carotid artery disease and stenosis, which, moreover, has a sizable contribution to the probability of developing an ischemic stroke[38,39]. Animals were trained to tolerate awake tail vein restraint for injection of tMP in days leading up to stroke, minimizing the effects of stress on stroke pathophysiology. Animals were briefly anesthetized

https://doi.org/10.1038/s41467-025-59617-1

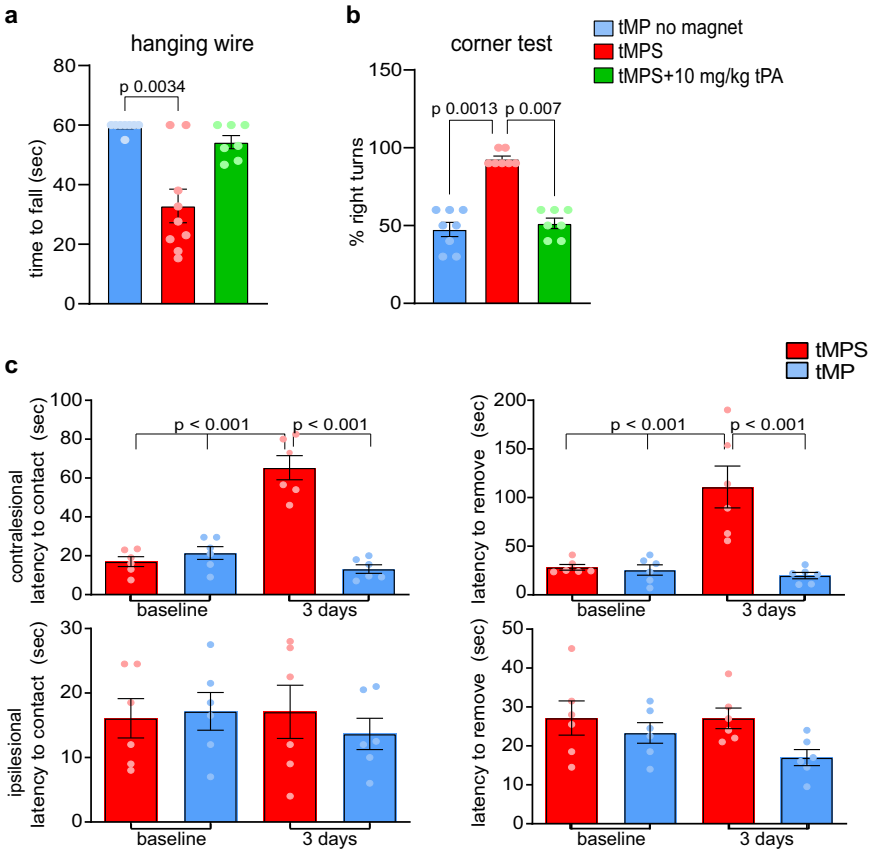

Fig. 3 | Motor-sensory impairment following tMP stroke. a Hanging wire test shows motor, grip strength, and balance impairments in MP stroke compared to sham mice at 48 h (*n*, sham = 8, tMPS = 9, tMPS + tPA = 7; Kruskal–Wallis with Dunn's post-hoc test). **b** Corner tests show sensorimotor perception impairments in MP stroke compared to sham at 48 h (sham *n* = 8, tMPS *n* = 7, tMPS + tPA *n* = 7; Kruskal–Wallis with Dunn's post-hoc test). **c** Time-to-contact and time-to-removal adhesive tape test between sham (receiving particles but no magnet) and stroke mice (particles and magnet). Notice significant increased time to remove adhesive at 3 days following stroke (*n* = 6/group; two-way ANOVA with Tukey's post-hoc test). All values are mean ± SEM. Source data are provided as a Source Data file.

for coil and magnet placement before being allowed to recover for awake injection of particles (Fig. 5a). This roughly 25-min surgical procedure is not thought to provide animals with anesthetic preconditioning that would impact development of the infarct[16,40]. Compared to tMPS with temporary carotid ligation (method described above), tMPS with unilateral carotid stenosis (designated tMPS coil) resulted in similar infarct volumes (11.5 ± 1.9 vs. 8.2 ± 1.3 mm^3, $p > 0.05$) and behavioral outcomes (Fig. 5b). Longitudinal LSI imaging of the mice undergoing tMPS coil procedure showed similar reperfusion dynamics when compared to the tMPS animals (Fig. 5d).

Next, we compared infarct volumes produced by tMPS coil with anesthesia to tMPS coil in awake animals. We found that infarct volumes were significantly smaller with anesthesia than without anesthesia (Fig. 6a). Since clinical and experimental data indicate circadian variations in the magnitude of stroke injury and treatment[41–43], we induced stroke in daytime and nighttime. We found no significant infarct volume difference between day-time and night-time strokes in either anaesthetized or awake animals (Fig. 6a). Finally, surgery-to-injection time intervals showed no correlation between the groups receiving surgery first versus last and overall stroke volume (Fig. 6b, c). This, along with the longitudinal LSI data (Fig. 5c), indicates that the carotid stenosis and CBF reduction by micro-coil provides a stable drop in CBF within this time frame of 2–3 h from surgery to injection for the particles to aggregate appropriately.

Discussion

Despite recent progress in therapeutic interventions, ischemic stroke remains a major risk factor for death and long-term disability. While preclinical stroke models have been pivotal in elucidating pathomechanisms and identifying potential druggable targets, the translation of these findings into clinical therapies has largely failed. The majority of preclinical stroke studies in mice have been performed by transient intraluminal proximal MCA occlusion (tMCAo), which blocks blood flow to the entire MCA territory, and by permanent distal MCA occlusion (pMCAo) specifically targeting cortical MCA supply territories. While tMCAo can mimic reperfusion and is therefore preferred when modeling large vessel ischemic strokes in humans that have been recanalized by tPA treatment or mechanical thrombectomy, it also reduces blood flow to the lenticulostriatal arteries, leading to ischemic injury of basal ganglia, a condition rarely seen in large vessel ischemic strokes in humans[37,44]. The pMCAo model results in lesions restricted to the neocortex and is therefore a better mimic of ischemic MCA strokes in humans, but can't be reperfused by either pharmacologic or endogenous thrombolysis.

To address these limitations, several focal thrombotic and thromboembolic stroke models have been developed and performed in mice. These models include photothrombotic (PT) stroke, topical $FeCl_3$ application to the MCA, and intraluminal thrombin injections. Similar to the tMPS model we outlined here, the PT stroke model is minimally invasive but does not mimic large vessel occlusion and is characterized by endothelial injury and vasogenic edema. Moreover, the mechanism of thrombosis in this model is distinct from classical thrombus formation as they do not require the presence of platelets or activation of the classical coagulation cascade[45]. Meanwhile local application of $FeCl_3$ over the MCA requires craniotomy and produces a platelet-rich thrombus that is not responsive to tPA reperfusion[46].

https://doi.org/10.1038/s41467-025-59617-1

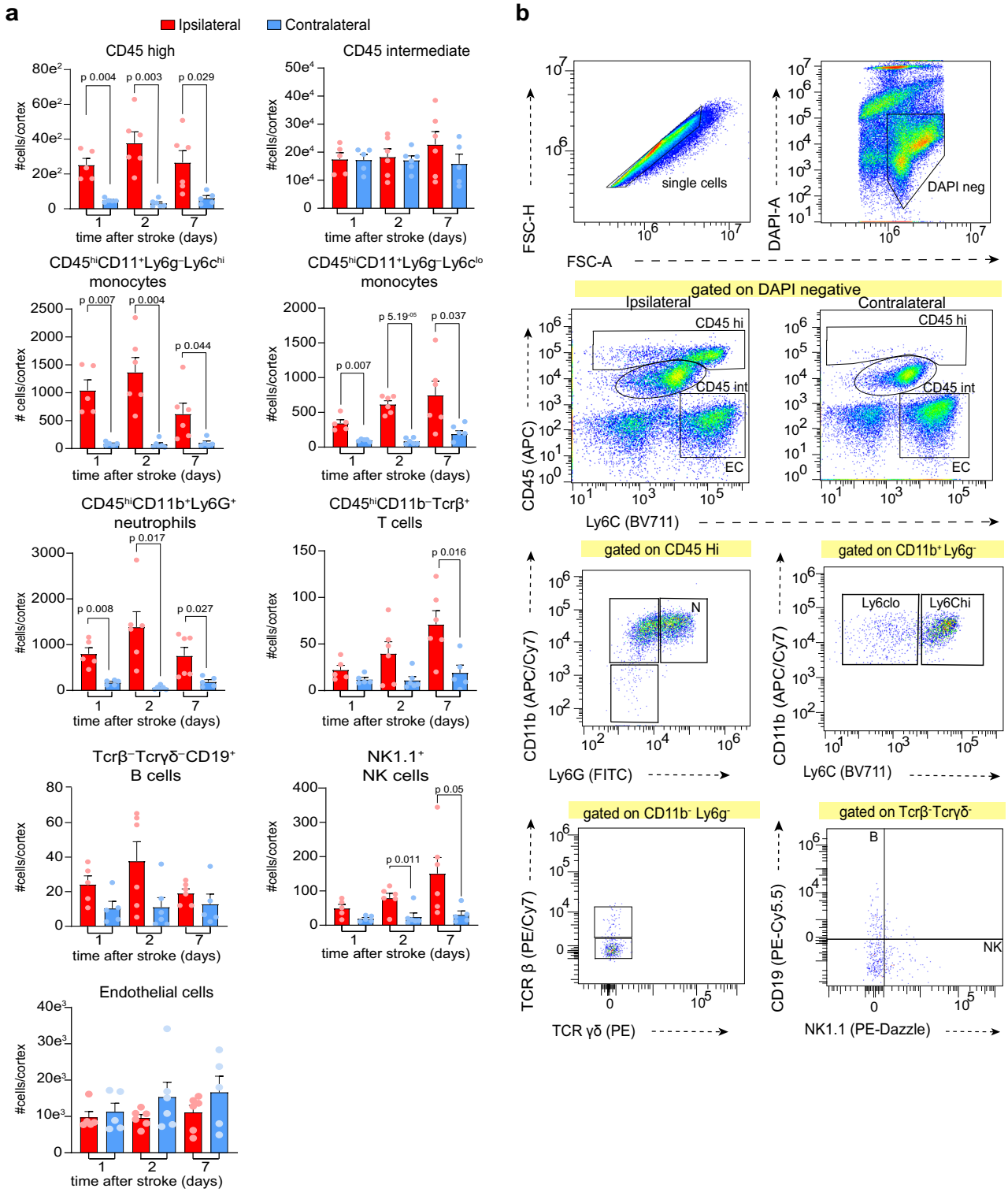

Fig. 4 | Longitudinal profile of immune cell infiltration after tMP stroke. Flow cytometry shows infiltration of peripheral immune cells after tMP stroke. **a** Cell counts for ipsi-and contralateral cortex at 1, 2, and 7 days following tMP stroke (1 d ipsi $n = 5$, 1 d contra $n = 5$, 2 d ipsi $n = 6$, 2 d contra $n = 6$, 7 d ipsi $n = 6$, 7 d contra $n = 5$; two-way ANOVA and unpaired two-sided t-test for hemisphere effects). Data are presented as mean values ± SEM. **b** Gating strategy flow scheme is shown for cortices at 2 days. Plots gated on DAPI$^-$ and CD45^{hi} compare both hemispheres. Subsequent plots below show ipsilateral cortex only. EC endothelial cells, N neutrophils, T T cells, B B cells, NK natural killer cells. Source data are provided as a Source Data file.

Intraluminal injection of thrombin into the MCA instead generates a thrombus that is composed of platelets and fibrinogen and, similar to the tMPS model, is amendable to tPA thrombolysis[47,48]. The surgical procedure, however, requires craniotomy, and the grade of clot formation is not consistent.

More recently, stroke models based on delivery of synthetic particles to the MCA or brain have been developed. Untargeted delivery of microspheres or cholesterol crystals via the CCA produces permanent microvessel occlusion, resulting in randomly distributed microinfarcts in cortical and subcortical brain regions that do not resemble large

https://doi.org/10.1038/s41467-025-59617-1

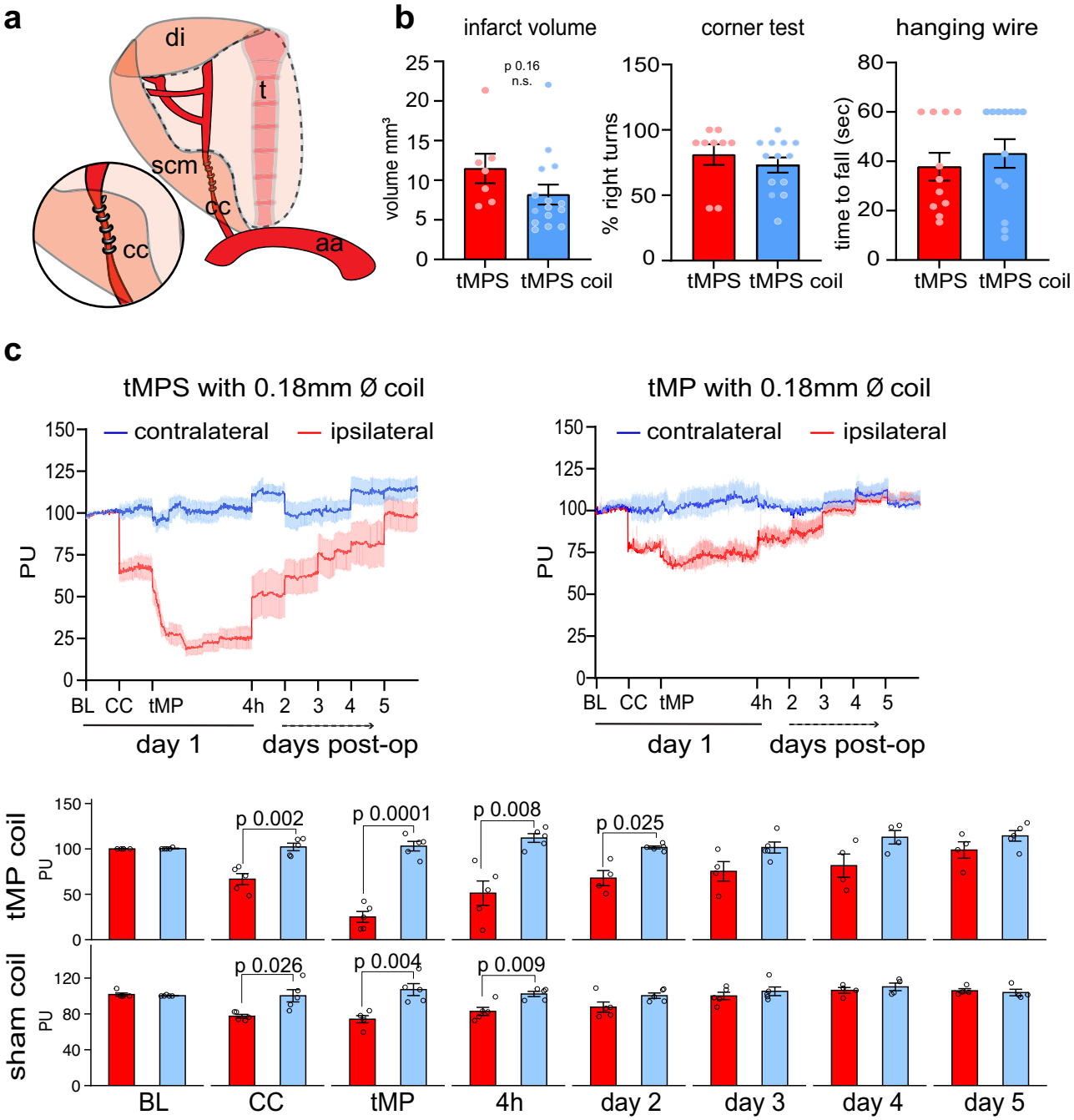

Fig. 5 | Optimization for awake stroke: tMP stroke using permanent unilateral coil and magnet. Animals underwent a short surgery (~25 min) under isoflurane (1.5%) for permanent placement of carotid coil and magnet (as outlined in methods), followed by injection of thrombin particles. **a** Instead of temporary ligation with nylon suture, animals received unilateral permanent placement of 0.18 mm Ø coil to the common carotid artery that is ipsilateral to cortex of intended injury and magnet placement (magnet left in place). di digastric muscle, scm sternocleidomastoid muscle, aa aortic arch, cc common carotid artery, t trachea. **b** 48-h infarct volume of tMPS compared to tMPS using coil both under anesthesia (tMPS $n = 7$, tMPS coil $n = 15$; unpaired two-sided t-test, p value). Forty-eight-hour corner and hanging wire behavior test between tMPS and tMPS using coil was not significant (corner test: tMPS $n = 9$, tMPS coil $n = 13$; hanging wire test: tMPS $n = 11$, tMPS coil $n = 13$; Mann–Whitney test). Data are presented as mean values ± SEM. **c** Animals were anesthetized (1.5% isoflurane) for surgery and LSI measurement. Animals were monitored for CBF as perfusion units (PU) following a baseline reading (BL), the unilateral coil placement on the carotid ipsilateral of permanent magnet placement (CC), following injection of particles and consequent tMP stroke (tMPS), 4 h following stroke, and up to 5 days. Sham animals followed identical surgical procedure and particle injection except for magnet placement (tMP). $n = 4$–5/group, unpaired two-sided t-test or Mann–Whitney test as appropriate. Data are presented as mean values ± SEM. Source data are provided as a Source Data file.

vessel strokes[43,49,50]. In contrast, magnetic nanoparticles can be directed to a determined vascular target by attractive magnet placement. The seminal study by Jia et al.[18] was based on the delivery of pegylated magnetic nanoparticles that were attracted to the MCA by a magnet placed on the skull, and this model has also been adapted for use in neonatal mice[51]. Subsequently, several other studies using magnetic nanoparticles, some of them modifications of the original protocol, have emerged. One such study used 100 nm thrombin-linked magnetic particles attracted to an NdFeB magnet placed on the CCA[52]. Upon clot formation and removal of the magnet, the thrombus embolizes to the

https://doi.org/10.1038/s41467-025-59617-1

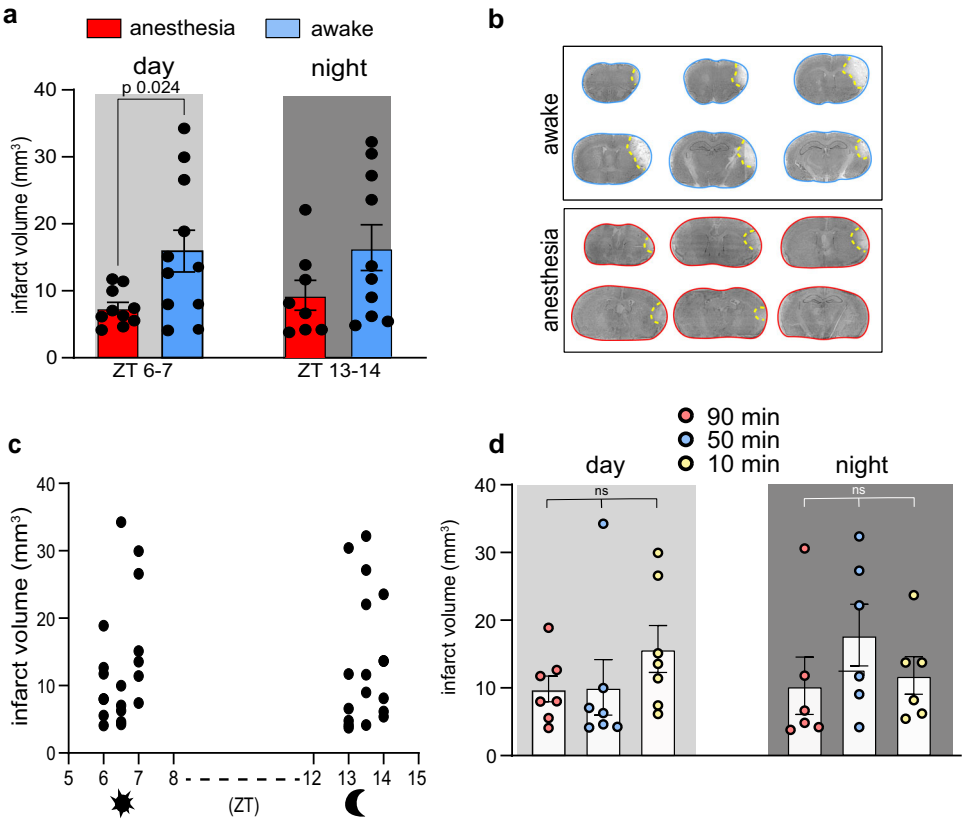

Fig. 6 | Effects of anesthesia and circadian cycle on tMP stroke. a Coil and magnet placement surgeries were performed mid-morning and injected as one group (in order of surgeries) at zeitgeber times (ZT) 6-7 or at (ZT) 13-14 (anesthesia (ZT6-7) $n = 10$, awake (ZT6-7) $n = 10$, anesthesia (ZT13-14) $n = 8$, awake (ZT13-14) $n = 10$; 2-way ANOVA). **b** Representative cresyl violet staining shown of 48 h post awake daytime coil tMPS, (top) outlined in blue and 48 h post isoflurane anesthetized daytime coil tMPS (bottom) outlined in red. Infarct territory outlined in yellow. **c** Paired time-to-particle injection following coil and magnet surgery. Animals were injected in the order of surgery, completed within 1–2 h of full recovery ($n = 6$/group). **d**, Infarct volumes of mice shown as time from end of surgery to particle injection (day $n = 7$, night = 6; Kruskal–Wallis test shows no effect of time between surgery and stroke induction). Individual values and mean ± SEM are shown. Source data are provided as a Source Data file.

MCA, leading to vessel occlusion. To date, no data are available detailing the extent of the ischemic territory, infarct volumes, reproducibility, or the response to rtPA. A second study made use of magnet placement on the MCA paired with magnetized red blood cells in P0-7 pups modeling perinatal cerebral hemorrhage and stroke[53]. Most recently, another group used magnetic particles to induce infarcts to the MCA P6 pups and P28 mice[54]. While these studies show promise and confirmation of what we see to be powerful tool using nanoparticles for modeling cerebral ischemia, neither is modeling thrombotic stroke in awake adult mice. Additional comparisons made between experimental models are shown in Supplementary Table. 2.

The tMPS model of stroke has several advantages over existing models. First, and most compelling, this model allows for stroke to occur in awake, non-anesthetized mice. The initial method development made use of anesthesia to validate and compare against the existing metrics of CBF, behavior, and the inflammatory response of the established models, which also use isoflurane. However, the model has been adapted to introduce MCA occlusion while the animal is fully conscious.

Modeling MCA stroke in non-anesthetized mice has long been a goal of the field and would eliminate the potentially confounding neuroprotective impact of inhalant anesthetics[16,17,55,56]. Awake ischemic strokes in rodents have been studied previously using intravascular filament[57], endothelin-1[58–61], photothrombotic[56,62,63], embolic strokes[64], and nanoparticles[18], but this awake model is the first to allow for thrombotic large artery occlusions in awake mice without craniotomy. It offers other technical benefits to experimenters: for example, it allows investigators to conduct strokes during the animal's wake cycle, having prepared the animals during the surgeons' daytime work hours and inject with tMP early evening at the start of the mouse's wake cycle without needing to perform stroke surgeries at nighttime. This allows for modeling morning-onset strokes frequently seen in humans[41,42,65–67] with ease to experimenters. Placing a coil around the carotid and a magnet over a thinned temporal bone requires roughly 20 min of surgery time, with the injection itself taking no more than 1–2 min to accomplish, and several animals can be injected with tMP all at once, as a batch. In contrast to surgery under anesthesia that requires an average of 50–60 min minimum to complete (namely due to requiring surgeons to wait 30 min following injection of the particles before removing the magnet and reversing the ligation), preparing animals for awake strokes ultimately saves time. We can't exclude that the transient increase in body temperature, heart rate, and plasma corticosterone levels, which can occur as a reaction to restraint stress[68], could affect stroke induction in awake mice and therefore contribute to the higher variability in awake strokes. However, changes of these physiologic parameters observed upon restraint stress are transient and they return to baseline values within 1 h[68]. It is therefore unlikely that these changes will affect the central pathophysiologic mechanisms, such as neuronal cell death and immune responses, downstream of the thrombotic occlusion.

The use of anesthesia in preclinical models of stroke has been a concern, given that anesthesia modulates the very molecular pathways known to be relevant in stroke[69,70]. All models deemed to provide awake strokes in rodents—including this one—require some duration

of anesthesia for the surgical preparation of animals before stroke. While anesthetics are still unavoidable, extra considerations should be taken for the duration and breadth of anesthesia prior to stroke induction to avoid preconditioning effects[71–73].

A major finding of this study is that infarct volumes were significantly smaller in tMPS animals with micro-coils injected under anesthesia compared to those injected awake, possibly indicating protective effects of anesthesia. No differences were seen in the infarct volumes or outcomes of these two groups when comparing strokes performed during the active or inactive cycle. Because of the high variance of infarct volumes in awake strokes (67% CV), we cannot exclude that our study was underpowered to detect more nuanced changes in the susceptibility to ischemic brain injury depending on the circadian cycle. In addition, our studies were limited to two circadian time brackets (ZT 6-7 and ZT 13-14), which might be insufficient to unravel the complexity of the circadian cycle and its effects on stroke outcome.

Animals under anesthesia undergoing tMPS either by temporary carotid ligation or by permanent coil placement resulted in similar infarct volumes and behavioral outcomes (Fig. 5a, b). Interesting to note is that following the permanent placement of a micro-coil, the magnet and after particle injection, reperfusion to the affected MCA closely matched what was seen with the reversible ligation and magnet removal in anesthetized mice, indicating that for an infarct to occur the magnet and carotid stenosis either by coil or ligation does not need to be removed after particle injection and that reperfusion occurs regardless of their removal (Fig. 5d).

This endogenous reperfusion is another marked advantage of the magnetic stroke model. Spontaneous recanalization and vascular patency after several days is a characterized phenomenon that occurs in stroke patients who do not undergo rtPA treatment[13,44]. Additionally, human ischemic stroke often has partial spontaneous reperfusion after endogenous dissolution of the thrombus within the first 48 h following stroke[12,13]. In a study following patients with MCA strokes by transcranial doppler within 6 h of infarct and at 1 week, more than half of the patients had normal flow to the MCA by 7 days, with 3 to 9 months follow-ups showing the same findings[74]. This is similar to the reperfusion pattern being shown by this model.

While it is not possible to compare the local amounts of thrombin to active thrombin endogenously generated in other models or human stroke, the spontaneous reperfusion observed in this model suggests that the delivered amounts of thrombin can be counteracted by the endogenous fibrinolytic system, suggesting that thrombin doses are within the "physiologic" range. However, the direct effects of thrombin on protease-activated receptors expressed on endothelial cells[75], leukocyte chemotaxis, endothelial barrier dysfunction, complement activation[76,77], and neurotoxicity[78] should be considered when interpreting studies using this model.

Large vessel atherosclerosis and carotid stenosis are the largest contributors to the pathophysiology of thromboembolic stroke to the MCA, accounting for most stroke cases in humans[38,39,79]. Logically, the primary cause of injury is relevant to the treatment of acute ischemic stroke in humans, thus, animal models should also be able to address this issue. The magnetic particle model models thrombotic stroke with the injection of occlusive particles into mouse circulation, allowing for aggregation of thrombin particles in a clot-like fashion to the MCA below the attractive magnet. It also has the capacity to model carotid stenosis using a unilateral carotid micro-coil.

Our studies following injection of tMP, measuring blood gases, liver enzymes, and cytokines, showed minimal impact to overall physiological parameters in mice. Iron (II, III) oxide particles have been used as imaging agents in humans, providing good biocompatibility and negligible toxicity[80]. Dextran and iron oxide magnetic nanoparticles, in particular, have been used for diagnostic imaging and therapeutics for cancer in humans[81,82].

Given the increased interest in the roles of meninges regulating brain function and the inflammatory response after stroke[83–85], the tMPS model, not needing craniotomy and compatible with in vivo imaging, is ideally suited to address their roles in the response to thrombotic stroke. The overall profile of infiltrating immune cells observed over 7 days post stroke in this model is comparable to the profiles reported for transient and permanent MCA occlusion models, showing an early increase of myeloid cells (neutrophils and monocyte-derived cells) with late participation of T and NK cells[31,86].

There are several limitations to this model. First, the largest limitation of the tMP stroke model is technical. While commonly done, injection by tail vein can be a challenge for new surgeons. One should be very proficient in injecting by tail vein (particularly in awake mice) before starting to perform the technique. Second, the coefficient of variation (CV) in infarct volumes of strokes performed under anesthesia was comparable to the one of the intraluminal filament stroke model routinely performed in our laboratory (31.9% vs 31.2% CV). However, the CV was 67% in the awake stroke group, which renders the awake model less suitable for drug discovery or genetic studies when effect sizes are small. Part of this variability might be attributed to the fact that CBF, which failed to drop sufficiently in 11% of animals in the anesthesia tMPS group (Supplementary Table 1), cannot be monitored in awake mice, and insufficient CBF reduction could contribute to the variation in infarct volumes. Third, in accordance with previous investigations into the biodistribution of magnetic nanoparticles[19,20], we found that tMP accumulated in sinusoidal Kupffer cells of the liver for at least up to 4 weeks without entering the liver parenchyma. While we could not detect histological or metabolic changes indicative of liver dysfunction or inflammation, the threshold for tMP toxicity could be lower in models with impaired liver function, including diabetes or high-fat diet. While there is a possibility of transient increase in total serum iron, previous studies have found that high doses of magnetite nanoparticles did not affect the serum iron binding capacity[87,88], making it unlikely that "free iron", a possible source of ROS formation, will be generated. This study did not address brain-blood barrier disruption, edema formation, and post-ischemic angiogenesis, important aspects of ischemic brain injury and repair. More studies are needed to establish how tMPS affects vascular integrity and restoration. Finally, while we show equal performance of the model in male and female mice, we did not test the model in different age groups. Although we did not observe sex effects on infarct volumes produced by this model, the current study might have been underpowered to reach a final conclusion, and more comprehensive studies should address the role of sex in the future.

Large vessel atherothrombosis accounts for ~20% of all human strokes[89], but modeling thrombotic strokes in rodents has remained challenging. The current models require craniotomy and are not suitable to be performed in conscious animals[90]. Here we present a model of thrombotic stroke of the distal MCA territory leading to reproducible cortical infarcts that does not require craniotomy, can be performed in awake mice, is amendable to rtPA reperfusion, and shows neurobehavioral and immune response characteristics similar to the ones reported for more invasive distal MCA occlusion models. We hope that the tMP stroke model will close some gaps in modeling human stroke in the preclinical setting.

Methods

Animals

8–12 week old C57Bl/6J male mice from JAX Laboratories were used for all studies. Where indicated, 19–24 week old C57Bl/6J female mice were used. Mice were housed socially (three to five mice per cage) in individually ventilated cages, with *ad libitum* access to food and water and under controlled conditions (22 ± 2 °C, 12:12 h light/dark cycle with light phase from 7:00 a.m. to 7:00 p.m.; 40–60% humidity). Mice from the same cage were subjected to stroke or sham surgeries, alternating,

respectively, and returned for recovery. Post-surgery sham and stroke mice were housed together (2–3 mice) in an environmental incubator at 31 °C, the thermoneutral temperature for mice[91,92], until study endpoint. Surgical success and attrition are presented in Supplementary Table 1. All experiments were performed under approved Institutional Animal Care and Use Committee protocol (Weill Cornell Medicine, #2012-0051) in accordance with National Institutes of Health guidelines and with the United States Public Health Service's Policy on Human Care and Use of Laboratory Animals. Results are reported according to ARRIVE[93] guidelines.

Magnetic particle size and composition

We used magnetic particles that are a composite of magnetite [iron(II, III) oxide] and 40 kDa dextran matrix (Nanomag-D, 180 nm or 500 nm, 10 mg/ml, MicroMod, Germany, Cat No. 09-82-182 and 09-00-502). When paired with a Neobydium attractive magnet (1.59 × 0.79 mm thick N52 NdFeB axially magnetized Ni coated magnet, Zigmyster magnets Cat No. D116-132N52) placed on the temporal bone, particles accumulated to the MCA after intravenous tail vein injection. Particles were rinsed with a magnetic pull-down rack three times using physiological saline and resuspended in 250 μl to make 10 mg/ml. Particles were sonicated in a water bath for 10 min immediately prior to injection.

Thrombin composite particles (tMP)

Custom order nanoparticles (MicroMod Nanomag-D, albumin (BSA), 500 nm, 10 mg/ml) were conjugated to bovine thrombin (Millipore) to induce clot formation. 20 U bovine thrombin (Millipore Sigma Cat No. 605157) in 0.1% BSA was added directly to aliquoted doses of 250 μl suspended magnetic particles and incubated overnight at 37 °C. Following incubation and using a magnetic bead separation rack, supernatant was discarded, and particles were rinsed twice using 300 μl saline and collected by magnetic pull down. Thrombin nanoparticles were resuspended in 250 μl of physiological saline and sonicated in a bath sonicator for 10 min before injection. The dose of thrombin conjugated to nanoparticles was determined by a coagulation assay. 5 U thrombin increments were added to microcentrifuge tubes containing 50 μl of human citrated plasma (Sigma Cat No. P9523-1ML) and the time to clot formation was recorded. The same 5 unit increments of thrombin were added to magnetic nanoparticles (250 μl) and incubated overnight at 37 °C. After washing the particles, human citrated plasma (Sigma Cat No. P9523) was added, and time to clot formation was recorded.

Magnetic particle model of stroke

Mice were anaesthetized with isoflurane (4.5–5% induction, 1.5% maintenance). Bupivacaine 0.25% solution was administered transdermally prior to any incision at both scalp and neck. Toe-pinch reflex was done to check for anesthetic depth. Body temperature was maintained at 37 °C using a feedback rectal probe and heating pad.

Reversible CCA ligation. With animal supine, a 1 cm incision was done to shaved and sterilized neck skin over trachea, without cutting trachea or muscles. Using sterile cotton swab soaked with saline, neck muscles were gently separated to reveal trachea and surrounding vessels. The right CCA was isolated using sterile micro-forceps. Care was taken not to disturb the vagus nerve, which can be seen as a fine white strand behind the carotid. Once the vessel was isolated, a 10 cm long 6-0 US silk surgical suture was fed below the carotid. Both ends of the suture were left loose and open until ready to inject particles. Mouse is then flipped over to the prone position for magnet placement.

Magnet placement. To a sterilized and shaved scalp, a 1–1.5 cm midline incision was made using sterile scissors and forceps. On the stereotaxic setup, the mouse head was rotated 40–45° to reveal the right temporal muscle. Using fine scissors and forceps, the margin where the temporal muscle attaches to the skull bone was cut, and the flap of temporal muscle was carefully retracted to expose the temporal bone below. Bleeding was controlled using sterile cotton swabs and frequent flushes of saline. As the supraorbital vein and retro-orbital sinus sit right along this margin, surgeons were mindful of extensive resection to avoid excessive bleeding. The branches of the MCA were visible, climbing upward from behind the zygomatic arch, below the temporal bone. A 2 mm area was thinned over the main trunk and distal branches of the MCA using a dental drill equipped with a ¼ mm drill burr on medium to low speed. Alternating every few seconds with saline-soaked cotton swabs to remove bone powder and to prevent overheating of the skull by drilling, the skull over the trunk of the MCA was thinned as close to the zygomatic arch as possible, using rapid strokes and light pressure while holding the drill bit nearly parallel to the bone. The skull is sufficiently thinned to 70 μm once the vessel is clearly visible without the addition of saline. The attractive magnet (1.59 × 0.79 mm thick N52 NdFeB axially magnetized Ni coated magnet; Zigmyster magnets Cat No. D116-132N52) was placed flat over the thinned region and glued down using Loctite gel superglue. Ideally, the magnet was placed on the ascending trunk of the MCA, and any probe measuring CBF was placed on downstream branches or just adjacent to the magnet on the trunk of the vessel, but further downstream if no branches were visible. Note that for reperfusion of vessel, the magnet and glue could be easily lifted by forceps.

Particle delivery and MCA occlusion. While the animal is still in the prone position, and immediately before injection of particles, the CCA was temporarily ligated by gently pulling on the implanted silk sutures and taping the ends to the stereotaxic setup, so both strings were taut. CBF reduction of ~25% is expected here. Thrombin-BSA conjugated particles suspended in physiological saline were sonicated for 10 min prior to delivery. Warm water was used to dilate the mouse tail vein, followed by an ethanol surgical wipe to the tail immediately prior to injection. Using a 1 ml syringe and 30 G needle, 250 μl (2.5 mg particles/mouse) sonicated particles were injected by tail vein. To monitor effective drop in blood flow, Doppler flowmetry (Perimed) or Laser Speckle Flowmetry (Omegazone) was used to record a sustained CBF decrease of 85% or greater for 30 min.

After 30 min, the CCA was released from ligation, and magnet was removed gently by forceps. The ligation was loosened by cutting the two tense, taped silk sutures. If continuously monitoring CBF, one can carefully slide the remaining relaxed suture out from under the carotid, still in the prone position, slowly using forceps. If not measuring blood flow, animal can be flipped to the supine position to slide out remaining suture from behind carotid. Animal was then closed for recovery using 6.0 USP nylon suture string on the neck and sterile wound clips on the scalp. Lidocaine topical analgesic was applied to surgical sites. A prepared, clean, warm cage is equipped with wet food and gauze for recovery. Animals are placed in a physiologic recovery chamber (Darwin chambers, 31 °C) for a minimum of 48 h and up to 7 days until ready to image or be euthanized. Following surgery, Buprenorphine at 0.5 mg/kg is administered every 6–8 h subcutaneously for the first 72 h following stroke.

Sham animals underwent the identical surgery to the tMP stroke groups, including skull thinning and transient CCA ligation, without placement of the attractive magnet. Sham animals were injected with either magnetic thrombin nanoparticles (tMP) or physiological saline as indicated.

Note. Investigator may opt to use rodent ear-bars to stabilize the animal's head during surgery, however, it is not absolutely necessary for this procedure, and strict use of the stereotax and ear-bars may impede in surgical flexibility as the head will be rotated by about 40°, making proper placement of the bars a challenge. Adding hand stabilization techniques, however, most comfortable for the surgeon, was

found to be most beneficial in avoiding errors during surgery, particularly with thinning the temporal bone and magnet placement.

Awake stroke procedure

Prior to surgery, mice were acclimated to a tail vein restrainer by 1 week of handling by researchers once daily for 5 min each. Handling is defined by holding mice, stroking fur and tail, and allowing animals to climb on hands of researchers. Handling is followed by 4 days of placing animals individually into the tail vein restrainer for 1 min.

Unilateral CCA stenosis by coil. Animals were anesthetized (Isoflurane induction 4–5%, maintained at 1.5%). Transdermal Bupivacaine 0.25% solution is administered to neck and scalp prior to incision. With animal supine and using sterile surgical technique, a 1 cm incision was done on shaved and cleaned skin over trachea, without cutting trachea or muscles. Using sterile cotton swabs with saline, neck muscles were pulled apart to reveal trachea and surrounding vessels. Right CCA was isolated, and a 10 cm long 4-0 US silk surgical suture was fed below the rostral segment of carotid. A 0.18 mm coil (Sawane Spring, Cat.No. SWP-A 0.18) was placed around the carotid, using the surgical suture to maneuver the vessel around the coil. Once the coil was properly placed around the CCA, the surgical suture was pulled out from below the carotid. CBF measurement using LSI over the surface of the skull and comparing to the contralateral hemisphere was done to confirm a 25% drop in CBF as a result of the carotid stenosis. Once confirmed, the neck skin is re-sutured with the coil left in place and lidocaine applied. Flipped to the prone position, the magnet was glued over a thinned temporal bone in the same technique outlined in the tMP stroke procedure. Once the magnet is well-glued, the scalp is closed using wound clips. Lidocaine was applied over incisions. Once fully ambulatory and exhibiting normal feeding and grooming behavior (by 1–2 h), mice were prepared for tMP injection as described, with the exception that mice were injected by tail vein while awake. Prior to tail vein injection, 0.25% bupivacaine was injected at the base of the tail, and topical lidocaine was applied over the length of the tail. Once in the restrainer, the mouse tail was carefully warmed (e.g., with a heat lamp or warm water) to cause vasodilation, increasing ease of vascular access. Once veins were clearly visible and dilated, 250 μl (10 mg/ml) of sonicated magnetic BSA-thrombin particles in saline was injected using a 1 ml syringe and 30 G needle. Following particle injection, animals were immediately placed in a warmed cage and soon after transferred to a designated regulated physiologic recovery chamber. Following surgery, Buprenorphine at 0.5 mg/kg was administered every 6–8 h subcutaneously for the first 72 h following stroke.

Circadian experiments

Mice underwent the awake stroke procedure at one of two dedicated times in a 12-h period. Mice had surgery mid-morning or late afternoon, followed by tMP injection 1–2 h later. Dedicated stroke (tMP injection) times were at either Zeitgeber time (ZT) 6–7 during their sleep inactive cycle (mid-day) or ZT 13–14 during their wake active cycle (early evening). Mice were injected as a group following recovery from surgery. "Anesthesia" mice underwent the same surgery outlined for the awake stroke procedure of coil and magnet placement and allowed to recover, but instead underwent anesthesia a second time for tMP injection for 10 min during the same dedicated Zeitgeber times. As in previous studies, mice were immediately placed in a warmed cage and transferred to a regulated recovery chamber, and following surgery, Buprenorphine was administered at a dose of 0.5 mg/kg every 6–8 h. Mice were euthanized 48 h later and assessed for stroke volume using Nissl staining.

Assessing systemic distribution of tMP by magnetic resonance imaging

Magnetic resonance imaging (MRI) was performed on a BioSpec 70/30 USR 7.0 Tesla Small Animal MRI at the Citigroup Biomedical Imaging Center (Weill Cornell Medicine) with a 200 mT/m gradient amplitude, a 640 mT/m/s slew rate, and a 20 cm inner bore diameter. Whole body T1 isotropic, T2 weighted, and T2Star mapping was done in animals injected with saline, tMP, and 30 min following tMPS. Animals were anaesthetized with 1.5–2% isoflurane during imaging. Raw DICOM data was processed using Fiji Image J software.

Assessment of physiological tolerance of magnetic particles in vivo

Femoral artery catheterization was performed to collect arterial blood for pCO_2, pO_2, and pH measurement in tMPS and tMP sham-injected animals before and following injection (Siemens Epoc Blood Analyzer System) ($N = 5$/group). Animals were under 1.5% isoflurane anesthesia. Arterial pressure was recorded by femoral artery catheterization using a pressure transducer (ADInstruments PowerLab data acquisition system and ADInstruments LabChart software for analysis). Given, the T2-weighted MRI images revealed accumulation of particles to the liver, liver serum chemistry was done at 4 h, 24 h, 48 h, and 7 days for alkaline phosphatase, alanine transaminase, aspartate transaminase, total serum protein, triglycerides, and total bilirubin by collecting blood from cheek puncture. Serum chemistries were performed by the Center of Comparative Medicine and Pathology at Memorial Sloan Kettering Cancer Center[94]. Serum levels of MCP-1, MIP1α, IL-4, IL-10, IL-6, IL-1β, IP-10, RANTES, and TNFα were measured by an U-PLEX multiplex assay (Meso Scale Diagnostics, custom order) and read by a MesoScale plate reader. Blood was collected by terminal cardiac puncture from stroke, particle sham, and saline groups at 4 h, 24 h, 48 h, and 7 days after intervention, and serum was obtained by centrifugation.

Cerebral blood flow measurement

Day of surgery, CBF was measured using Laser Doppler Flowmetry (LDF). Downstream flow from the distal branches of the MCA was measured using an optical fiber paired with the Perimed Master Probe 418. The fiber/probe was placed with the flat tip of the fiber flush on the temporal bone over the vessel downstream of the magnet. Both the glued fiber/attached probe and magnet remained glued on the temporal bone for the entirety of blood flow recording. Pairing (Loctite) gel glue and (Insta-set) glue accelerator was necessary to facilitate precise placement. Laser Doppler was continuously measured to give recordings at baseline, during the tMP injection/occlusion, and magnet removal/reperfusion. Raw data files were normalized to a baseline value of 100, and every 5 s of linear recording was averaged using a custom R script. Data was plotted for the corresponding 5 min baseline recording, 10 min carotid ligation, 30 min occlusion, and 30 min reperfusion performed in surgery. Linear recordings were binned to reflect an average for each time segment for each animal and plotted as bar graphs. Note that occlusion and reperfusion groups were binned using the last 10 min of recordings, and this segment was used for statistics.

LSI was also used to measure whole brain spatial and temporal dynamics of CBF to both hemispheres during tMP stroke and in the days following to model reperfusion to the MCA after the magnet is removed[95]. These longitudinal imaging experiments were performed with an Omegazone OZ-2 Laser Speckle Tissue Blood Flow Imager with laser unit and CCD camera. Anesthetized animals (1.5–2% Isoflurane) were prepared for tMP stroke as described above, including the nylon suture placed behind the CCA and magnet placement, prior to preparing the skull for LSI.

Prior to imaging, whole skull thinning was performed with the dental drill. With animal securely attached to ear bars in the stereotaxic table and scalp still open from previous magnet placement, scalp and white periosteum were trimmed laterally to expose the entire dorsal surface of the skull. Scalp skin was glued to edges using Vetbond. Note that the temporal muscle was already removed for the placement of

the magnet, and the magnet will still need to be removed for MCA reperfusion. This side of the scalp was left partially unglued until procedure was finished, and tissue glue on this side was added when animal was ready to move to recovery. Thinning of the skull to ~90 μm thickness on both hemispheres was done to resolve the MCA for imaging. Daily repeated thinning was needed to control for bone regrowth as animals were imaged for several days. Prior to imaging, bacteriostatic light scattering gel was applied using a cotton swab. The gel is removed using a cotton swab, and a sterile saline rinse is applied to clean the surface of the skull before the animal can recover. LSI was done longitudinally, providing recordings at baseline, during the CCA ligation, magnetic particle injection/occlusion, and magnet removal/reperfusion. Animals were re-anesthetized and imaged up to 5 days following surgery. For each time point, LSI images were obtained every 1 s for duration of the procedure. Frames with significant artifacts obscuring the MCA were deleted, and LSI images were averaged over 1 min per each time point and, using Fiji ImageJ software, a region of interest was drawn around the major MCA branch on each corresponding cortex and compared with the identical region on the contralateral side, measuring changes in pixel intensity.

Nissl staining for infarct volume measurement

Brains were prepared fresh and flash-frozen in an isopentane bath. Cryostat (Leica CM1850) slices of coronal sections at 30 μm thickness were collected every 250 μm. Sections were fixed in 4% paraformaldehyde in 0.1 M phosphate buffer for 10 min. Following fixation, sections were rinsed in 0.1 M phosphate buffer for 5 min and then incubated in Cresyl Violet solution for 12–15 min. Sections were then placed in water for 2 min before dehydration in sequential baths of 50%, 75%, 95%, and 100% ethanol, 10 s each. Sections were cleared in two sequential 2-min incubations of Xylene before mounting with DPX permanent mounting solution. Infarct volume determination was done using ImageJ software. Using the freehand selections tool in ImageJ, the perimeter of infarct was traced, and area was measured and converted to mm^3. The contralateral hemisphere was used to correct for edema by applying the formula $\text{infarct volume}_{\text{corrected}} = \text{infarct volume}_{\text{measured}} - (\text{volume of ipsilateral hemisphere} - \text{volume of contralateral hemisphere})$[14].

Liver histology

Mice were deeply anesthetized using sodium pentobarbital (150 mg/kg, i.p.) and transcardially perfused with ice-cold Phosphate Buffered Saline (PBS) and 2% Paraformaldehyde (PFA) fixative. Fixed tissues were processed in ethanol and xylene and embedded in paraffin in a Leica ASP6025 automated tissue processor (Leica Biosystems, Buffalo Grove, IL, USA). Paraffin blocks were sectioned at 5 μm thickness with a microtome, sections were mounted on glass slides, and stained with hematoxylin and eosin (H&E) on a Leica Autostainer XL and coverslipped on a Leica CV5030 coverslipper. Whole slide images were acquired with an Olympus VS200 slides scanner and VS200 ASW 4.4.1 software (Evident Scientific, Hamburg, Germany) using a 40X/0.95NA objective to generate whole slide images with a pixel size of 0.1369 μm. Kupffer cells were putatively identified by their location in liver sinusoids, by exhibiting a large pale soma with high proportion of vacuolization.

Immunohistochemistry

At 2, 7, and 14 days following stroke, animals were deeply anesthetized using sodium pentobarbital (150 mg/kg, i.p.) and transcardially perfused with ice cold PBS and 2% PFA fixative. Isolated brains were kept at 4 °C in the 2% PFA overnight before moving to 30% Sucrose for 2 days. Eighteen-micrometer sections were cut by cryostat (Leica CM1850). Sections were rehydrated with 1X PBS and permeabilized using 0.5% PBS-T (Triton X100) for 30 min. Next, sections were blocked for 2 h in 5% normal donkey serum in 0.1% PBS-T. Sections were incubated in 0.1% PBS-T, 1% normal donkey serum and with corresponding primary antibodies for 2 days at 4 °C. Primary antibodies included anti-MAP2 (1:200, rabbit polyclonal, abcam Cat. No ab32454), anti-Iba1 (1:500, rabbit polyclonal, Wako Sigma Aldrich Cat No. SAB5701363), anti-GFAP (1:200, rabbit polyclonal, abcam Cat. No ab7260). Primary antibodies were removed by washing sections twice with 1X PBS for 5 min. Sections were incubated for 2 h at room temperature, shielded from light in 1% normal donkey serum, 0.5% PBS-T, and corresponding secondary antibodies in FITC goat anti-rabbit (abcam Cat. No ab6717), Cy5 goat anti-rabbit (Thermofisher Cat. No A10523), or Cy3 goat anti-rabbit (Thermofisher Cat. No A10520) at 1:100. Sections were washed twice with 1X PBS for 5 min. Sections were mounted using Fluorosave containing DAPI (Sigma-Aldrich Cat No. F6057).

Immunostaining using anti-fibrinogen antibody (rabbit anti-mouse polyclonal, abcam Cat. No ab34269) and antibody for platelet marker CD41 (rat anti-mouse, Biolegend Cat. No 133903) of the distal branches of the MCA and embedded clot was done on a vibratome-cut 40 μm free-floating coronal sections. Brain sections were selected from 24-well storage container and rinsed with 0.1 M phosphate buffer to remove agar from vibratome. Sections were washed with 1X PBS twice for 5 min and then permeabilized with 0.5% PBS-T for 1 h at room temperature. Sections were washed with 1X PBS twice for 5 min. Sections were then blocked with 3% normal donkey serum in 0.5% PBS-T for 1 h at room temperature. Sections were washed twice with 1X PBS for 5 min. Sections were left in primary antibodies 1:500 anti-fibrinogen and 1:500 anti-CD41 overnight in 0.5% PBS-T at 4 °C. Sections were washed with 1X PBS the following day. Secondary antibodies, Cy3 goat anti-rabbit (Thermofisher Cat. No A10520) and FITC goat anti-rat (ThermoFisher Cat No. 31629), were incubated at 1:100 for 2 h in 0.5% PBS-T at room temperature, shielded from light. Floating sections were washed thoroughly with 1X PBS and mounted on slides. Slides and sections were allowed to dry before mounting coverslips using FluoroSave (Sigma-Aldrich F6057).

Fluorescent activated cell sorting

Mice were anesthetized with sodium pentobarbital (150 mg/kg, ip) intraperitonial. Single cell suspensions of mouse cerebral cortex were prepared after transcardial cold PBS (containing 2U/ml Heparin) perfusion. The entire cerebral cortex was dissected and placed into tubes containing 2 ml digestion solution (HBSS, 10 mM Hepes pH 7.4, 1 mM $MgCl_2$, 50 U/ml DNAse I) on ice. Once all brains were collected, 50 μl of Dispase (Worthington Cat No. 2104, 32 U/ml) and 50 μl Liberase DH (Roche Cat No. 12352200, 2.5 mg/ml) were added to each sample. Tissues were homogenized using a tissue dissociator (gentleMACS, m_brain_01 program, Miltenyi Biotech). Samples were then placed in an orbital shaker for 45 min at 37 °C at 100 rpm. Tissues were again homogenized using a tissue homogenizer (gentleMACS, brain_03 program) and transferred to 15 ml Falcon tubes on ice. Samples were centrifuged at 1000 × *g* for 10 min at 4 °C. Pellets were resuspended 1 ml in 30% Percoll (Cytiva Cat. No 17089101) in HBSS/HEPES and resuspended 25 times using a p1000 pipette. 9 ml of 30% Percoll was then added to each sample, mixed by inversion, and samples were spun at 1750 rpm for 15 min at 4 °C. Myelin was removed by aspiration using a Pasteur pipette. Supernatant was removed, and pellets were individually resuspended in 10 ml HBSS/HEPES. Samples were spun at 1000 × *g* for 7 min at 4 °C. Supernatant was discarded, and pellets were each resuspended in 1 ml FACS (2% Fetal Bovine Serum, 0.05% NaN_3 in 1x PBS) buffer into FACS tubes. 3 ml of FACS buffer was then added to each sample, and samples were spun at 1500 rpm for 6 min at 4 °C. Supernatant was discarded, and samples were blocked in 50 μl FACS buffer containing CD16/CD32 (Biolegend Cat No. 101301, Clone 93, 5 ng/μl) for 10 min. Samples were then stained with 5 μl of corresponding antibody mix. The following antibodies and channels were used to differentiate leukocyte populations CD4 BV510 (Biolegend Cat. No 100553, Clone RM4-5, 0.16 ng/μl), CD45 APC (Biolegend Cat. No 103111, Clone 30-F11, 0.6 ng/μl), Ly6C BV711

(Biolegend Cat. No 128037, Clone HK1.4, 0.39 ng/μl), TCRγδ PE (Biolegend Cat. No 118107, Clone GL3, 0.39 ng/μl), CD8a AF700 (Biolegend Cat. No 100729, Clone 53-6.7, 0.08 ng/μl), NK1.1 PE-Dazzle (Biolegend Cat No. 108747, Clone PK136, 0.64 ng/μl), CD19 PE-Cy5.5 (Thermofisher Cat No. RM7718, Clone 6D5, 0.5 ng/μl), TCRβ PE-Cy7 (Biolegend Cat No. 109222, Clone H57-597, 0.39 ng/μl), Ly6G FITC (Biolegend Cat No. 127605, Clone 1A8, 1 ng/μl), CD11b APC/Cy7 (Biolegend Cat No. 101226, Clone M1/70, 0.08 ng/μl). Samples were stained for 15 min on ice and washed in 3 ml of FACS buffer. Samples were spun for a final time at 1500 rpm for 7 min at 4 °C and then resuspended in 200 μl of FACS for sorting. Samples were acquired on a NovoCyte Quanteon flow cytometer and analyzed using FlowJo version 10.7 software. Discrimination gates were established using isotype controls and fluorescence minus one experiments.

Neurological deficits

Behavior tests were performed to measure the functional neurological deficits of mice following tMP stroke. Animals underwent hanging wire and corner test recordings[27]. Two days following injury, mice are suspended on an outstretched, taut wire between two poles roughly 60 cm above the ground or table. Mice must initially grab the wire with both fore-paws and allowed to "hang" and are given 60 s to reach either of the two poles. The "latency to fall" is the amount of time the animal can remain suspended without falling. After 1 min, the trial is over. Animals reaching either pole are automatically given a score of 60 s for the trial. Three trials are performed for each mouse with 10 min intervals. The corner test was used to establish sensorimotor deficits and motor asymmetries following injury. The testing setup included two darkened walls angled at 30° to a corner. At the junction of the two walls, a small amount of light should be allowed to pass through, and food pellets can be placed behind the walls to motivate the animal to enter the corner. Animals are placed between the two walls and allowed to approach the corner and then rear upwards, both palms on the wall, and turn back around. Investigators record the direction of rearing/turning. Trials in which the animal does not rear upward while turning are discarded. Each animal performs 10 consecutive trials. Animals also performed the adhesive removal test at 3 days following stroke for assessment of sensorimotor deficits[30]. Animals receive two adhesive tape strips to their forepaws and are timed for 120 s in a clear testing box equipped with a camera. Contact time is defined as the point at which the mouse recognizes the presence of the tape strips (ex., shaking paws or touching tape to the mouth). Removal of the first and second pieces or tape is recorded for the moment the tape touches the bottom of the clear container. Animals were trained 3 days before stroke to establish a baseline reading and re-tested at 3 days following stroke.

Adaptation of tMP stroke for multiphoton imaging

All steps of the surgical preparation for magnetic particle stroke were done prior to preparing the skull with a thin-skull window for imaging. The original scalp incision, which was done for magnet placement, was elongated as needed to expose the entire occipital bones. Using forceps and surgical scissors, the periosteum was trimmed laterally to the edges of the temporal bone. Scalp skin was glued to the edge of where the temporal muscle inserts onto the temporal bone and the tissue on the posterior of the neck using Vetbond tissue glue, exposing whole dorsal skull surface. Note that one will have already removed parts of the temporal muscle for placement of the magnet and may choose to remove the magnet after the 30-min occlusion. Therefore, this portion of the scalp remains open until imaging procedure is finished and the animal is ready to move to recovery. Vetbond can be used to close the scalp. Mice are secured in the stereotaxic setup prior to thinning and placing the headplate using rodent ear bars. Using a ½-mm burr on medium to low speed, the parietal bone was lightly thinned on the ipsilateral side of the occlusion to slightly flatten the area where the headplate will be added. The skull was swabbed every few seconds with a saline-soaked cotton swab to avoid overheating and remove bone fragments. The distal branches of the MCA are visible in C57Bl/6J mice ascending below the surface of the temporo-parietal bone, roughly perpendicular to where the magnet was placed over the MCA on the temporal bone. A 2-mm by 2-mm region was mapped over where the vessel is seen under the parietal bone. Investigators thinned through the cancellous layer of bone in this 2-mm by 2-mm region using low drill speed and feather-light strokes, always alternating every few seconds with saline and cotton swabs. At the point where the pial vessels are visible under moist saline-soaked bone, white spots in the spongey bone layer will show on the surface of the skull. The area was continuously thinned until these spots disappeared, indicating the inner plate of the parietal bone has been exposed. Extreme care is taken here not to apply unnecessary pressure and avoid overheating of the bone. At this point, a small droplet of cyanoacrylate glue was added over the thinned area, and a 2-mm round glass coverslip was placed flat over the glue. The glue and coverslip will prevent bone re-growth and imaging aberrations during chronic imaging studies. If imaging once, the thin-skull window can be left bare and submerged in water when imaging. After coverslip placement, a custom headplate was affixed with dental cement (C&B Metabond, Parkell) to the lateral aspect of the parietal bone just superior to the temporal bone[96]. The headplate was positioned with the screw points facing laterally, roughly perpendicular to the temporal bone, leaving the temporal bone and glued-on magnet below clean of dental cement. Dental cement was built up in a circle around the coverslip to prevent bone re-growth, allowing cement to slightly dry and thicken before placing the titanium headplate.

Two-photon imaging of mice undergoing tMP stroke

Mice were kept anesthetized with 1.2–1.5% isoflurane in mixed oxygen and nitrogen to target a ~1 Hz respiratory rate while keeping the core body temperature at 37 °C with a feedback-controlled heating pad. Mice were stabilized by attaching the headplate to a metal frame on an optical breadboard. 70 kDa Texas Red-conjugated dextran (50 μl, 2.5% w/v dissolved in saline, Invitrogen) was injected retro-orbitally to visualize the vasculature just prior to imaging. Leukocytes and blood platelets were labeled with Rhodamine 6 G (0.1 ml, retro-orbitally, 1 mg/ml in 0.9% saline, Acros Organics). Hoechst 33342 dye was also injected retro-orbitally (50 μl, 4.8 mg/ml in 0.9% saline, Thermo Fisher Scientific) to label leukocytes and distinguish them from platelets. Before imaging, the surface of the coverslip was gently cleaned with a moist cotton swab. Red blood cell speed and vessel diameter changes were monitored at baseline, following CCA ligation, during injection of tMP, and following removal of magnet and CCA ligation. These steps were done while the mouse was secured to the imaging setup. Animals' neck tissue was re-sutured following imaging, and the mouse was allowed to recover in ambient stroke recovery chamber for future imaging.

Imaging was performed on a two-photon microscope (FVMPE, Olympus). Excitation pulses came from a solid-state (InSightDS+ Spectraphysics) laser at 820 nm. Fluorescence was collected through band-pass emission filters (Hoechst, 410–460 nm; Rhodamine 6 G, 495–540 nm; Texas Red, 575–645 nm) and delivered to photomultiplier tubes. All image stacks were collected using Fluoview software (Olympus), where each hyperstack movie consists of the three fluorescent layers. To visualize brain architecture and identify distal branches of the MCA, a 300 μm deep wide field map was taken using a 5X objective (0.28 NA, Olympus). Once the MCA branch had been identified, we used a water-submerged 25X objective (SLPlan N 1.05 NA, Olympus) to perform all line scans and acquire z-stacks. Red blood cell velocity was measured by repetitive unidirectional scans across the central axis of the vessel at 0.85 kHz for 60 s. Red blood cells were seen as diagonal dark streaks. The slope of these individual streaks is inversely proportional to blood cell speed. Scans were analyzed using

MATLAB code with a Radon transform-based algorithm computing line integrals of the $g(x, y)$ 2D image at various angles[97]. All remaining images and movies were processed using ImageJ software.

Statistical analysis

Data was analyzed for normal distribution using the Shapiro-Wilk normality test. Group-wise comparisons were performed with two-tailed *t*-test, one- and two-way ANOVA, or Kruskal–Wallis test as appropriate. Statistical analysis was performed using Prism 10 (GraphPad Software, RRID:SCR_002798) and the R statistical environment (RRID:SCR_001905).

Reporting summary

Further information on research design is available in the Nature Portfolio Reporting Summary linked to this article.

Data availability

Data supporting the findings of this study are available in the article, its Supplementary Information, and the Source Data file. Additional data is available at https://doi.org/10.6084/m9.figshare.28625153 and from the corresponding authors upon request. Source data are provided with this paper.

Code availability

Analysis code is available at https://doi.org/10.6084/m9.figshare.28625153.

References

1. Virani, S. S. et al. Heart disease and stroke statistics—2020 update: a report from the American Heart Association. *Circulation* **141**, e139–e596 (2020).
2. Campbell, B. C. V. et al. Ischaemic stroke. *Nat. Rev. Dis. Prim.* **5**, 70 (2019).
3. Virani, S. S. et al. Heart disease and stroke statistics—2021 update. *Circulation* **143**, e254–e743 (2021).
4. Bhaskar, S., Stanwell, P., Cordato, D., Attia, J. & Levi, C. Reperfusion therapy in acute ischemic stroke: dawn of a new era? *BMC Neurol.* **18**, 8 (2018).
5. Hussein, H. M. et al. Occurrence and predictors of futile recanalization following endovascular treatment among patients with acute ischemic stroke: a multicenter study. *AJNR Am. J. Neuroradiol.* **31**, 454–458 (2010).
6. Xu, H. et al. Predictors of futile recanalization after endovascular treatment in patients with acute ischemic stroke in a multicenter registry study. *J. Stroke Cerebrovasc. Dis.* **29**, 105067 (2020).
7. Ter Schiphorst, A. et al. Tissue no-reflow despite full recanalization following thrombectomy for anterior circulation stroke with proximal occlusion: a clinical study. *J. Cereb. Blood Flow. Metab.* **41**, 253–266 (2021).
8. Aroor, S. R. et al. Mechanical thrombectomy access for all? Challenges in increasing endovascular treatment for acute ischemic stroke in the United States. *J. Stroke* **24**, 41–48 (2022).
9. Xian, Y. et al. Achieving more rapid door-to-needle times and improved outcomes in acute ischemic stroke in a nationwide quality improvement intervention. *Stroke* **53**, 1328–1338 (2022).
10. Bacigaluppi, M., Comi, G. & Hermann, D. M. Animal models of ischemic stroke. Part two: modeling cerebral ischemia. *open Neurol. J.* **4**, 34–38 (2010).
11. Prinz, V. & Endres, M. in *Rodent Models of Stroke* (ed Ulrich Dirnagl) 19-29 (Springer, 2016).
12. Toni, D. et al. Early spontaneous improvement and deterioration of ischemic stroke patients. A serial study with transcranial Doppler ultrasonography. *Stroke* **29**, 1144–1148 (1998).
13. Kassem-Moussa, H. & Graffagnino, C. Nonocclusion and spontaneous recanalization rates in acute ischemic stroke: a review of cerebral angiography studies. *Arch. Neurol. Chic.* **59**, 1870–1873 (2002).
14. Jackman, K., Kunz, A. & Iadecola, C. Modeling focal cerebral ischemia in vivo. *Methods Mol. Biol.* **793**, 195–209 (2011).
15. Molina, C. A. et al. Timing of spontaneous recanalization and risk of hemorrhagic transformation in acute cardioembolic stroke. *Stroke* **32**, 1079–1084 (2001).
16. Koerner, I. P. & Brambrink, A. M. Brain protection by anesthetic agents. *Curr. Opin. Anesthesiol.* **19**, 481–486 (2006).
17. Jickling, G. C. & Sharp, F. R. Improving the translation of animal ischemic stroke studies to humans. *Metab. Brain Dis.* **30**, 461–467 (2015).
18. Jia, J. M. et al. Control of cerebral ischemia with magnetic nanoparticles. *Nat. Methods* **14**, 160–166 (2017).
19. Lunov, O. et al. Lysosomal degradation of the carboxydextran shell of coated superparamagnetic iron oxide nanoparticles and the fate of professional phagocytes. *Biomaterials* **31**, 9015–9022 (2010).
20. Portilla, Y. et al. Different coatings on magnetic nanoparticles dictate their degradation kinetics in vivo for 15 months after intravenous administration in mice. *J. Nanobiotechnol.* **20**, 543 (2022).
21. Park, L. et al. The key role of transient receptor potential melastatin-2 channels in amyloid-β-induced neurovascular dysfunction. *Nat. Commun.* **5**, 5318 (2014).
22. Doll, D. N., Barr, T. L. & Simpkins, J. W. Cytokines: their role in stroke and potential use as biomarkers and therapeutic targets. *Aging Dis.* **5**, 294–306 (2014).
23. Ferrarese, C. et al. Increased cytokine release from peripheral blood cells after acute stroke. *J. Cereb. Blood Flow. Metab.* **19**, 1004–1009 (1999).
24. Bonaventura, A. et al. Update on inflammatory biomarkers and treatments in ischemic stroke. *Int. J. Mol. Sci.* **17** https://doi.org/10.3390/ijms17121967 (2016).
25. Lambertsen, K. L., Biber, K. & Finsen, B. Inflammatory cytokines in experimental and human stroke. *J. Cereb. Blood Flow. Metab.* **32**, 1677–1698 (2012).
26. Iadecola, C. & Anrather, J. The immunology of stroke: from mechanisms to translation. *Nat. Med.* **17**, 796–808 (2011).
27. Balkaya, M., Kröber, J. M., Rex, A. & Endres, M. Assessing post-stroke behavior in mouse models of focal ischemia. *J. Cereb. Blood Flow. Metab.* **33**, 330–338 (2013).
28. Suenaga, J. et al. White matter injury and microglia/macrophage polarization are strongly linked with age-related long-term deficits in neurological function after stroke. *Exp. Neurol.* **272**, 109–119 (2015).
29. Zhang, L. et al. A test for detecting long-term sensorimotor dysfunction in the mouse after focal cerebral ischemia. *J. Neurosci. Methods* **117**, 207–214 (2002).
30. Bouet, V. et al. The adhesive removal test: a sensitive method to assess sensorimotor deficits in mice. *Nat. Protoc.* **4**, 1560–1564 (2009).
31. Gelderblom, M. et al. Temporal and spatial dynamics of cerebral immune cell accumulation in stroke. *Stroke* **40**, 1849–1857 (2009).
32. Iadecola, C., Buckwalter, M. S. & Anrather, J. Immune responses to stroke: mechanisms, modulation, and therapeutic potential. *J. Clin. Investig.* **130**, 2777–2788 (2020).
33. Manglani, M. & McGavern, D. B. Intravital imaging of neuroimmune interactions through a thinned skull. *Curr. Protoc. Immunol.* **120**, 24.22.21–24.22.12 (2018).
34. Shih, A. Y. et al. Two-photon microscopy as a tool to study blood flow and neurovascular coupling in the rodent brain. *J. Cereb. Blood Flow. Metab.* **32**, 1277–1309 (2012).
35. Drew, P. J. et al. Chronic optical access through a polished and reinforced thinned skull. *Nat. Methods* **7**, 981–984 (2010).
36. Denny, M. C. et al. Wake-up Strokes Are Similar to Known-Onset Morning Strokes in Severity and Outcome. *J. Neurol. Neurol. Disord.* **1** https://doi.org/10.15744/2454-4981.1.102 (2014).

37. Sommer, C. J. Ischemic stroke: experimental models and reality. *Acta Neuropathol.* **133**, 245–261 (2017).
38. Flaherty, M. L. et al. Carotid artery stenosis as a cause of stroke. *Neuroepidemiology* **40**, 36–41 (2013).
39. Rothwell, P. M. et al. Analysis of pooled data from the randomised controlled trials of endarterectomy for symptomatic carotid stenosis. *Lancet* **361**, 107–116 (2003).
40. Eltzschig, H. K. & Eckle, T. Ischemia and reperfusion-from mechanism to translation. *Nat. Med.* **17**, 1391–1401 (2011).
41. Lo, E. H. et al. Circadian biology and stroke. *Stroke* **52**, 2180–2190 (2021).
42. Reidler, P. et al. Circadian rhythm of ischaemic core progression in human stroke. *J. Neurol. Neurosurg. Psychiatry* **94**, 70–73 (2023).
43. Ryu, W. S. et al. Association of ischemic stroke onset time with presenting severity, acute progression, and long-term outcome: a cohort study. *PLoS Med.* **19**, e1003910 (2022).
44. Carmichael, S. T. Rodent models of focal stroke: size, mechanism, and purpose. *NeuroRx* **2**, 396–409 (2005).
45. Stoll, G., Kleinschnitz, C. & Nieswandt, B. Molecular mechanisms of thrombus formation in ischemic stroke: novel insights and targets for treatment. *Blood* **112**, 3555–3562 (2008).
46. Martinez de Lizarrondo, S. et al. Potent thrombolytic effect of N-acetylcysteine on arterial thrombi. *Circulation* **136**, 646–660 (2017).
47. Orset, C. et al. Mouse model of in situ thromboembolic stroke and reperfusion. *Stroke* **38**, 2771–2778 (2007).
48. El Amki, M. et al. Experimental modeling of recombinant tissue plasminogen activator effects after ischemic stroke. *Exp. Neurol.* **238**, 138–144 (2012).
49. Silasi, G., She, J., Boyd, J. D., Xue, S. & Murphy, T. H. A mouse model of small-vessel disease that produces brain-wide-identified microocclusions and regionally selective neuronal injury. *J. Cereb. Blood Flow. Metab.* **35**, 734–738 (2015).
50. Wang, M. et al. Focal solute trapping and global glymphatic pathway impairment in a murine model of multiple microinfarcts. *J. Neurosci.* **37**, 2870–2877 (2017).
51. Jia, J. M., Peng, C., Wang, Y., Zheng, J. & Ge, W. P. Control of occlusion of middle cerebral artery in perinatal and neonatal mice with magnetic force. *Mol. Brain* **11**, 47 (2018).
52. Li, H., Yang, Z., Tang, Q., Shi, Z. & Mao, Y. Embolic stroke model with magnetic nanoparticles. *ACS Appl. Mater. Interfaces* **13**, 43993–44001 (2021).
53. Jin, Y. et al. Precise control of embolic stroke with magnetized red blood cells in mice. *Commun. Biol.* **5**, 136 (2022).
54. Lan, Y. et al. Fate mapping of Spp1 expression reveals age-dependent plasticity of disease-associated microglia-like cells after brain injury. *Immunity* **57**, 349–363.e349 (2024).
55. Kirsch, J. R., Traystman, R. J. & Hurn, P. D. Anesthetics and cerebroprotection: experimental aspects. *Int Anesthesiol. Clin.* **34**, 73–93 (1996).
56. Seto, A. et al. Induction of ischemic stroke in awake freely moving mice reveals that isoflurane anesthesia can mask the benefits of a neuroprotection therapy. *Front Neuroenergetics* **6**, 1 (2014).
57. Xie, L., Kang, H. & Nedergaard, M. A novel model of transient occlusion of the middle cerebral artery in awake mice. *J. Nat. Sci.* **2**, e176 (2016).
58. Bogaert, L. et al. Neurochemical changes and laser Doppler flowmetry in the endothelin-1 rat model for focal cerebral ischemia. *Brain Res.* **887**, 266–275 (2000).
59. Gelb, A. W., Bayona, N. A., Wilson, J. X. & Cechetto, D. F. Propofol anesthesia compared to awake reduces infarct size in rats. *Anesthesiology* **96**, 1183–1190 (2002).
60. Callaway, J. K., Knight, M. J., Watkins, D. J., Beart, P. M. & Jarrott, B. Delayed treatment with AM-36, a novel neuroprotective agent, reduces neuronal damage after endothelin-1-induced middle cerebral artery occlusion in conscious rats. *Stroke* **30**, 2704–2712 (1999).
61. Stoop, W. et al. Post-stroke treatment with 17beta-estradiol exerts neuroprotective effects in both normotensive and hypertensive rats. *Neuroscience* **348**, 335–345 (2017).
62. Balbi, M. et al. Targeted ischemic stroke induction and mesoscopic imaging assessment of blood flow and ischemic depolarization in awake mice. *Neurophotonics* **4**, 35001 (2017).
63. Lu, H. et al. Induction and imaging of photothrombotic stroke in conscious and freely moving rats. *J. Biomed. Opt.* **19**, 96013 (2014).
64. Zhang, R. L. et al. Postischemic intracarotid treatment with TNK-tPA reduces infarct volume and improves neurological deficits in embolic stroke in the unanesthetized rat. *Brain Res.* **878**, 64–71 (2000).
65. Burns, E. R. Biological time and in vivo research: a field guide to pitfalls. *Anat. Rec.* **261**, 141–152 (2000).
66. Elliott, W. J. Circadian variation in the timing of stroke onset: a meta-analysis. *Stroke* **29**, 992–996 (1998).
67. Esposito, E. et al. Potential circadian effects on translational failure for neuroprotection. *Nature* **582**, 395–398 (2020).
68. Meijer, M. K., Spruijt, B. M., van Zutphen, L. F. M. & Baumans, V. Effect of restraint and injection methods on heart rate and body temperature in mice. *Lab. Anim.* **40**, 382–391 (2006).
69. Traystman, R. J. in *Rodent Models of Stroke* (ed. Ulrich Dirnagl) 123–146 (Springer, 2016).
70. Mosneag, I.-E., Flaherty, S. M., Wykes, R. C. & Allan, S. M. Stroke and translational research—review of experimental models with a focus on awake ischaemic induction and anaesthesia. *Neuroscience* S0306452223005353 https://doi.org/10.1016/j.neuroscience.2023.11.034 (2023).
71. Hoffmann, U., Sheng, H., Ayata, C. & Warner, D. S. Anesthesia in experimental stroke research. *Transl. Stroke Res.* **7**, 358–367 (2016).
72. Mergenthaler, P., Dirnagl, U. & Meisel, A. Pathophysiology of stroke: lessons from animal models. *Metab. Brain Dis.* **19**, 151–167 (2004).
73. Wen, Z. et al. Optimization of behavioural tests for the prediction of outcomes in mouse models of focal middle cerebral artery occlusion. *Brain Res.* **1665**, 88–94 (2017).
74. Zanette, E. M. et al. Spontaneous middle cerebral artery reperfusion in ischemic stroke. a follow-up study with transcranial Doppler. *Stroke* **26**, 430–433 (1995).
75. Rezaie, A. R. Protease-activated receptor signalling by coagulation proteases in endothelial cells. *Thromb. Haemost.* **112**, 876–882 (2014).
76. Amara, U. et al. Interaction between the coagulation and complement system. *Adv. Exp. Med. Biol.* **632**, 71–79 (2008).
77. Ye, F., Garton, H. J. L., Hua, Y., Keep, R. F. & Xi, G. The Role of Thrombin in Brain Injury After Hemorrhagic and Ischemic Stroke. *Transl. Stroke Res.* **12**, 496–511 (2021).
78. Chen, B. et al. Thrombin activity associated with neuronal damage during acute focal ischemia. *J. Neurosci.* **32**, 7622–7631 (2012).
79. Kerwin, W. S. Carotid artery disease and stroke: assessing risk with vessel wall MRI. *ISRN Cardiol.* **2012**, 180710 (2012).
80. Karimi, Z., Karimi, L. & Shokrollahi, H. Nano-magnetic particles used in biomedicine: core and coating materials. *Mater. Sci. Eng. C. Mater. Biol. Appl.* **33**, 2465–2475 (2013).
81. Davis, M. E., Chen, Z. G. & Shin, D. M. Nanoparticle therapeutics: an emerging treatment modality for cancer. *Nat. Rev. Drug Discov.* **7**, 771–782 (2008).
82. McCarthy, J. R. & Weissleder, R. Multifunctional magnetic nanoparticles for targeted imaging and therapy. *Adv. Drug Deliv. Rev.* **60**, 1241–1251 (2008).
83. Herisson, F. et al. Direct vascular channels connect skull bone marrow and the brain surface, enabling myeloid cell migration. *Nat. Neurosci.* **21**, 1209–1217 (2018).

84. Simoes Braga Boisserand, L. et al. VEGF-C prophylaxis favors lymphatic drainage and modulates neuroinflammation in a stroke model. *J. Exp. Med.* **221,** e20221983 (2024).
85. Goertz, J. E., Garcia-Bonilla, L., Iadecola, C. & Anrather, J. Immune compartments at the brain's borders in health and neurovascular diseases. *Semin. Immunopathol.* **45**, 437–449 (2023).
86. Beuker, C. et al. Immune cell infiltration into the brain after ischemic stroke in humans compared to mice and rats: a systematic review and meta-analysis. *Transl. Stroke Res.* **12**, 976–990 (2021).
87. Bolandparvaz, A. et al. Biodistribution and toxicity of epitope-functionalized dextran iron oxide nanoparticles in a pregnant murine model. *J. Biomed. Mater. Res. A* **108**, 1186–1202 (2020).
88. Weissleder, R. et al. Superparamagnetic iron oxide: pharmacokinetics and toxicity. *Am. J. Roentgenol.* **152**, 167–173 (1989).
89. Petty, G. W. et al. Ischemic stroke subtypes: a population-based study of incidence and risk factors. *Stroke* **30**, 2513–2516 (1999).
90. Mosneag, I. E., Flaherty, S. M., Wykes, R. C. & Allan, S. M. Stroke and translational research - review of experimental models with a focus on awake ischaemic induction and anaesthesia. *Neuroscience* **550**, 89–101 (2024).
91. Gordon, C. J. *Temperature Regulation in Laboratory Rodents* (Cambridge University Press, 1993).
92. Karp, C. L. Unstressing intemperate models: how cold stress undermines mouse modeling. *J. Exp. Med.* **209**, 1069–1074 (2012).
93. Percie du Sert, N. et al. The ARRIVE guidelines 2.0: updated guidelines for reporting animal research. *J. Cereb. Blood Flow. Metab.* **588**, 271678X20943823 (2020).
94. Muscari, A. et al. Changes of liver enzymes and bilirubin during ischemic stroke: mechanisms and possible significance. *BMC Neurol.* **14**, 122 (2014).
95. Ayata, C. et al. Laser speckle flowmetry for the study of cerebrovascular physiology in normal and ischemic mouse cortex. *J. Cereb. Blood Flow. Metab.* **24**, 744–755 (2004).
96. Ahn, S. J., Anfray, A., Anrather, J. & Iadecola, C. Calcium transients in nNOS neurons underlie distinct phases of the neurovascular response to barrel cortex activation in awake mice. *J. Cereb. Blood Flow. Metab.* **43**, 1633–1647 (2023).
97. Santisakultarm, T. P. et al. In vivo two-photon excited fluorescence microscopy reveals cardiac- and respiration-dependent pulsatile blood flow in cortical blood vessels in mice. *Am. J. Physiol. Heart Circ. Physiol.* **302**, H1367–H1377 (2012).

Acknowledgements

We thank all members of the Anrather and Iadecola laboratories for helpful discussion. This work was supported by NIH grants R01NS081179 (J.A.), R01NS132493 (J.A.), and the Leducq Foundation (StrokeIMPaCT Network; J.A.). We also acknowledge the NIH/NCI Cancer Center Support Grant (P30 CA008748) for use of the Tri-Institutional Laboratory of Comparative Pathology, Memorial Sloan Kettering Cancer Center, Weill Cornell Medicine, and The Rockefeller University, and the Citigroup Biomedical Imaging Center at Weill Cornell Medicine for their technical assistance. The generous support of the Feil Family Foundation is gratefully acknowledged.

Author contributions

K.M. and J.A. conceived the study with the input of C.I. and K.M. performed the experiments and analyzed the data with contributions from S.A., A.A., N.R. and S.A. performed two-photon imaging and contributed to imaging analysis. A.A performed blood gas measurements. N.R performed some stroke experiments. K.M. and J.A. wrote the original draft. C.I. revised the manuscript. All authors read and approved the final manuscript.

Competing interests

C.I. serves on the scientific advisory board of Broadview Ventures. The other authors declare no competing interests.

Additional information

Supplementary information The online version contains supplementary material available at https://doi.org/10.1038/s41467-025-59617-1.

Correspondence and requests for materials should be addressed to Josef Anrather.

Peer review information *Nature Communications* thanks Woo-ping Ge and the other, anonymous, reviewer(s) for their contribution to the peer review of this work. A peer review file is available.